Postorogenic sediment drape in the Northern Pyrenees explained using a box model

Post-orogenic sediment drape in the Northern Pyrenees explained using a box model

Thomas Bernard[1], Hugh D. Sinclair[1], Mark Naylor[1], Frédéric Christophoul[2] and Mary Ford[3]

[1]*School of GeoSciences, The University of Edinburgh, Drummond Street, Edinburgh, EH8 9XP, United Kingdom.*

[2]*Université de Toulouse, Géosciences Environnement Toulouse, Toulouse, France.*

[3]*Centre de Recherches Pétrographiques et Géochimiques (CRPG), Université de Lorraine, Nancy, France.*

Acknowledgements

We thank Charlotte Fillon and Paul Angrand for discussions and early feedbacks. We thank Atle Rotevatn for editorial support and Peter van der Beek, Xiaoping Yuan and an anonymous reviewer for constructive comments, which allowed us to improve the manuscript. Finally, we thank the OROGEN project, a TOTAL-BRGM-CNRS consortium, for supporting this study.

Abstract

The transition to a post-orogenic state in mountain ranges has been identified by a change from active subsidence to isostatic rebound of the foreland basin. However, the nature of the interplay between isostatic rebound and sediment supply, and their impact on the topographic evolution of a range and foreland basin during this transition, has not been fully investigated. Here, we use a box model to explore the syn- to post-orogenic evolution of foreland basin/thrust wedge systems. Using a set of parameter values that approximate the northern Pyrenees and the neighbouring Aquitaine foreland basin, we evaluate the controls on sediment drape over the frontal parts of the retro-wedge following cessation of crustal thickening. Conglomerates preserved at approximately 600 m elevation, which is ~300 m above the present mountain front in the northern Pyrenees are ca. 12 Ma, approximately 10 Myrs younger than the last evidence of crustal thickening in the wedge. Using the model, this post-orogenic sediment drape is explained by the combination of a sustained, high sediment influx from the range into the basin relative to the efflux out of the basin, combined with cessation of the generation of accommodation space through basin subsidence. Post-orogenic sediment drape is considered a generic process that is likely to be responsible for elevated low-gradient surfaces and preserved remnants of continental sedimentation draping the outer margins of the northern Pyrenean thrust wedge.

Keywords

Northern Pyrenees, foreland basin, post-orogenesis, sediment drape, sediment flux.

Main Text

1. Introduction

Foreland basins are located at the outer edges of mountain belts (Dickinson, 1974). They are formed during mountain building and topographic growth. Flexure of the continental lithosphere is generated principally by topographic loads and controlled by the distribution of topography, internal density variations in the range and the flexural rigidity of the lithosphere (Beaumont, 1981; Jordan, 1981; Watts, 2001). The flexural basin forms the principle trap for sediments sourced from erosion of the neighbouring mountain range. Consequently, the stratigraphy, sedimentology and subsidence

history of foreland basins contain an integrated record of orogenesis (Sinclair, 2012). Foreland basins have a typical asymmetric cross-section with a greater thickness at the orogenic margin and a wedge-shaped form that tapers out over the stable craton. The cratonic margin of a foreland basin is generally defined by the distal pinchout of the basin stratigraphy onto the region of forebulge uplift. During orogenesis, as a mountain range grows by increases in both width and elevation, it is expected that a large proportion of eroded sediment is trapped in the foreland basin (Allen et al., 1986; Sinclair and Naylor, 2012). However, transition to an inactive decaying mountain range results in a reduction of the topographic load on the lithosphere and an associated isostatic rebound of foreland basins implying a bypass of sediment through the foreland basin to more distal depocentres (Burbank, 1992; Cederbom et al., 2004; Champagnac et al., 2007).

A well documented example is the pro-foreland Ebro foreland basin of the Pyrenean system (Vergés and Muñoz, 1990; Muñoz, 1992). The Ebro basin is characterized by a period of continental conglomeratic deposition linked to a rapid phase of exhumation in the Central Pyrenean Axial Zone during Late Eocene-Early Oligocene times as demonstrated by low-temperature thermochronological data (Fitzgerald et al., 1999; Sinclair et al., 2005). The sediments generated during this period caused thick accumulations in the Ebro Basin that draped the South Pyrenean Thrust Belt (Coney et al., 1996) as a result of tectonic confinement and endorheic conditions (Fillon et al., 2013). It has been proposed that piedmont aggradation for the Southern Pyrenees reduced the erosive capacity of rivers resulting in the development of high-elevation low-gradient surfaces within the internal zone of the belt (Babault et al., 2005a). The presence of low-gradient surfaces on both side of the range (Babault et al., 2005a, Bosch et al., 2016) has led to the proposal that similar processes were also active on the northern flank of the Pyrenees (Babault et al., 2005a). However, there is no evidence for basin confinement in the north. A regional climatic control on base-level rise and subsequent fall across the mountain chain is also discussed by (Babault et al., 2005a). Syn-tectonic conglomerates of the northern Pyrenees such as the Palassou and Toulouse Formations, were influenced by active structures of the Sub-Pyrenean Zone limiting their aggradation on the range. However, sedimentation continued during post-orogenesis with deposition of the undeformed Upper Carcassonne Group (i.e. Late Oligocene-Early Middle Miocene) which onlaps and seals structures of the northern Pyrenean flank (Serrano et al., 2006; Rougier et al., 2016; Ortiz et al., 2020). This raises the question of what controlled the accumulation of this drape during post-orogenic conditions (i.e. during isostatic rebound), and how this may have influenced the topography of the system.

Several studies have explored the effect of piedmont aggradation on the large-scale range topographic evolution by both numerical (Baldwin et al., 2003; Pelletier, 2004; Carretier and Lucazeau, 2005) or analogue modelling (Babault et al., 2005b; Babault et al., 2007). Experiments show that piedmont sedimentation plays an important role on the timescale of lowered denudation rates by reducing range relief and hillslope gradients at high altitude (Pelletier, 2004; Babault et al., 2005b). However, our understanding of why piedmont sedimentation occurs during the onset of post-orogenic isostatic rebound of the thrust wedge and foreland basin is unclear.

Underpinning the transition to a post-orogenic state is the competition between erosion and crustal thickening. The balance of these processes determines the timing and magnitude of isostatic rebound and hence subsidence versus uplift of the foreland basin. It is expected that any change in the parameters controlling the balance of erosion versus crustal thickening of the range will impact the general vertical movements, topographic evolution of the foreland basin and sediment flux into surrounding depocentres, for example, continental margins. In order to explore these interactions, we take full advantage of a simplification of the system represented in a box model that has been previously applied to the growth and decay of mountain belt/foreland basin systems (Tucker and van der Beek, 2013). In a series of experiments we simulate a counter-intuitive increase in sediment aggradation at the mountain front during the transition from syn- to post-orogenesis. We focus our analysis on the northern retro-wedge and retro-foreland Aquitaine Basin, and use this case study to define a range of parameter values for the model. We find a correlation between predicted post-orogenic sediment drape of the model, and the evidence of post-orogenic, late Miocene conglomerates draping the North

Pyrenean Frontal Thrust. We conclude that an initial signal of post-orogenic decay of mountain belt/foreland basin systems is the aggradation of coarse and proximal sediments draping the frontal parts of the thrust wedge without the need for external forcing such as sediment ponding or changes in climate.

2. Geologic setting of the Northern Pyrenees

2.1. Pyrenean tectonics

The Pyrenean mountain belt is a doubly-vergent collisional orogen that constitutes a westerly segment of the Alpine-Himalayan belt caused by the closure of the Tethys Ocean (Roure et al., 1989). The Pyrenees form a linear east-west orographic barrier (450 km-long and 150 km-wide) between Spain and France with a steep and wet flank in the Northern Pyrenees compared with a gentler and dryer flank in the Southern Pyrenees. Its formation results from convergence between the Iberian micro-plate and the European plate from late Cretaceous time (i.e. 84 Ma) to early Miocene time (i.e. 20 Ma) (Roest and Srivastava, 1991). The Pyrenean mountain belt can be divided into different tectonic units (Figure 1; Seguret, 1972; Muñoz, 1992; Vergés et al., 2002). The South Central Pyrenean Thrust Belt comprises three main thrust sheets (Sierra Marginales, Montsec and Boixols) of mainly Mesozoic carbonate platform and siliciclastic Paleogene rocks (Muñoz, 1992). The Axial Zone in the central and eastern Pyrenees, comprises thick Precambrian and Paleozoic metamorphosed sedimentary successions intruded by Variscan granitoid massifs (Vergés and Muñoz, 1990; Muñoz, 1992). The North Pyrenean Thrust Belt (NPTB) involves Variscan basement massifs and Mesozoic to lower Eocene sedimentary cover rock. Two foreland basins associated with the Pyrenean orogeny developed simultaneously: the Ebro pro-foreland basin (*sensu* Naylor and Sinclair, 2008) situated on the under-thrusting Iberian plate (Muñoz, 1992) and the Aquitaine retro-foreland basin situated on the over-thrusting European plate (Brunet, 1986; Bourrouilh et al., 1995).

Despite a large volume of research on the kinematic reconstruction of the Iberian plate with respect to the European plate, the total amount of shortening, the kinematics and timing and the rate of convergence are still a subject of debate (Beaumont et al., 2000; Mouthereau et al., 2014, Macchiavelli et al., 2017). Total amount of shortening of the Iberian plate indicates about 180 km of convergence (Olivet, 1996; Rosenbaum et al., 2002; Sibuet et al., 2004) and increasing from west to east (Vergés et al., 2002). However in the Central Pyrenees, different amounts of shortening have been proposed to interpret geological structures along the ECORS deep seismic line. Beaumont et al. (2000) estimates shortening of ~160 km compared with Roure et al., (1989) and Mouthereau et al. (2014) who respectively indicate 100 and 92 km of shortening across the Central Pyrenees. Macchiavelli et al. (2017) proposes a N-S shortening of 125 km.

Estimation of shortening rates also varies in the Central Pyrenees: Mouthereau et al., (2014) indicates that the most rapid shortening happened during the onset of convergence at 80-60 Ma (3.5 mm/yr) followed by a period of constant shortening at 2.0 mm/yr. In contrast, Beaumont et al., (2000) model an initial convergence from late Cretaceous to Eocene time of 2.0 mm/yr followed by an increase of shortening rate of 4 mm/yr during Oligocene time. Macchiavelli et al., (2017) proposes a more complex shortening rate history but in better agreement with the model of Beaumont et al., (2000) for the Cenozoic history. Grool et al., (2018) use cross-section restoration and subsidence analyses to quantify convergence rates and find good accordance with the convergence rates from Macchiavelli et al., (2017).

Following the main phase of orogenesis, the eastern Pyrenees and Aquitaine basin have been affected by extensional tectonics related to the opening of the Gulf of Lyon during Oligocene-Miocene time (Jolivet et al., 2015).

2.2. Exhumation of the central Pyrenees

The main phase of syn-orogenic exhumation in the Pyrenees has been documented in the Central Axial Zone and North Pyrenean Zone by an extensive data set of bedrock thermochronological ages (Figure 2). The first evidence of bedrock cooling was dated at about 55 Ma in the Northern Pyrenees using apatite and zircon fission track data (Yelland et al., 1990; Morris et al., 1998; Fitzgerald et al., 1999; Sinclair et al., 2005; Vacherat et al., 2016). The main phase of exhumation is recorded during Mid-Eocene and Oligocene times by apatite fission track and Apatite helium data (Fitzgerald et al., 1999; Sinclair et al., 2005; Gibson et al., 2007; Metcalf et al., 2009). The main cooling phase is diachronous in the Central Pyrenees with exhumation younging from north to south (Fitzgerald et al., 1999; Sinclair et al., 2005). This diachroneity is interpreted as the record of an initial phase of structural inversion in the Northern Pyrenees followed by the progressive migration of deformation toward the south. Inverse modelling of thermochronological data indicate that cooling slowed significantly after 30-25 Ma (Gibson et al., 2007; Bernard et al., 2019) with the latest cooling in the Barruera massif located in the southern Axial Zone, which records the growth of the antiformal stack from 36 to 20 Ma (Sinclair et al., 2005; Gibson et al., 2007). Young cooling ages (i.e. 10-20 Ma) record local late exhumation in the southern Pyrenees (Gibson et al., 2007; Jolivet et al., 2007). Inverse modelling of a compilation of zircon and apatite fission track and apatite helium ages (Bernard et al., 2019) indicate that the transition from syn-orogenic shortening to post-orogenic quiescence in the Central Pyrenees is also diachronous and youngs southward (Figure 2).

2.3. Stratigraphy of the Aquitaine Basin

As predicted by models of retro-foreland basin development (Naylor and Sinclair, 2008; Sinclair, 2012), the Aquitaine Basin preserves the full stratigraphic record of Pyrenean growth summarized in Figure 2 (adapted from Ford et al., 2016). Much of the western and central basin is superimposed on a pre-orogenic rifted crust. Sedimentation began during minor Permo-Triassic rifting between the Iberian and European plate; the sedimentary succession comprises red sandstones, evaporites and shallow marine deposits (Rougier et al., 2016). The Jurassic and Cretaceous periods were dominated by marine carbonate, marl and dolomite deposition (Biteau et al., 2006). During the principal rifting phase from Aptian to early Cenomanian a thick succession of deep marine clastics (Black Flysch group) and rim carbonates (Pierrelys group) was deposited in a series of distinct depocentres created under a transtensional regime (Debroas, 1990).

The Upper Cretaceous is dominated by marine flysch and marl sedimentation of the Grey Flysch Group deposited during post-rift thermal subsidence, followed by the Petites Pyrénées and Plantaurel Groups, which record accelerated subsidence during early convergence between the Iberian and European plates (Monod et al., 2014; Rougier et al., 2016; Ford et al., 2016). A period with low tectonic subsidence during the early Paleocene (i.e. 66-59 Ma) is recorded by continental clastic deposits in the east (Aude Valley Group) and westward younging shallow marine deposits (Rieubach group). A second phase of subsidence starting during late Palaeocene times is first recorded by a short -lived marine incursion from the west across the whole foreland basin. In the eastern Pyrenees, sedimentation became predominantly continental during late Ypresian time (Ford et al., 2016) with deposition of the Carcassonne Group, while marine conditions continued further west. This marine-continental transition migrated as the basin infill prograded westward. The Carcassonne Group comprises a continental succession of mudstones with variable volumes of conglomerates, sandstones and limestones. Conglomerates sourced from the orogen occur mainly in the Sub-Pyrenean Zone (SPZ), adjacent to the thrust front (Palassou Formation, Figure 2; Ford et al., 2016).

Post-orogenic stratigraphy of the Northern Pyrenees (i.e. latest Oligocene to Miocene times) is characterized by the upper Carcassonne Group (Rougier et al., 2016; Ford et al., 2015; including the Armagnac, Agenais and Toulouse Formations); these comprise a fine grained detrital continental succession consisting of carbonate-rich siltstones, marls, dolomites and limestones deposited in fluvial, palustrine and lacustrine environments (Ford et al., 2015). Micaschist and quartz-rich pebble to cobble conglomerates and mica-rich sandstones were deposited across the Sub-Pyrenean zone and along the

thrust front (Rougier et al., 2016). Across the whole Aquitaine platform the upper Carcassonne Group displays a high and constant thickness. The undeformed Upper Carcassonne Group onlaps eroded folds and reverse faults of the Sub-Pyrenean Zone and seals the Sub-Pyrenean Thrust and North Pyrenean Frontal Thrust (Figure 3). This indicates that the Sub-Pyrenean Thrust and North Pyrenean Frontal Thrust ceased to be active around late Oligocene - early Miocene time.

Miocene sediments of the Upper Carcassonne Group can be found in the foothills of the range (Figure 1, 2 and 4) from ~300 to ~600 m with a mean elevation of ~500 m. Sediment drapes that are thought to be of Miocene age are principally found on the central portions of the northern Pyrenees and correspond to the deposition of large alluvial fans. From west to east, Miocene sediments are found in the Adour, Lannemezan and Salat fans (Figure 4). Miocene sediments preserved along the Adour and Lannemezan fans show similar mean elevations of ~500 to ~550 m. The Lannemezan fan formed during middle to upper Miocene and Pliocene times and was abandoned when the Neste River was captured by the Garonne River during Quaternary times (Mouchené et al., 2017). Limited preservation of the Salat fan shows similar elevations to the Adour and Lannemezan fans, which suggests a similar mechanism of formation. As with the Lannemezan fan, the main stream network of the Salat fan was captured by the Garonne River. Miocene surfaces lying between the Lannemezan and Salat fan show lower mean elevations of ~400 m (Figure 4). These surfaces could reflect deposition in a relatively lowland area between two fans.

3. Methods

Our aim is to apply a parsimonious approach to the modelling of an orogenic system and associated foreland basin. Numerous models have been developed in order to investigate landscape evolution controlled by the coupling between tectonic deformation, flexural isostasy and surface processes. Two-dimensional models simulating mass transport from both fluvial and hillslope erosion through diffusive equations predict the relationship between thrust deformation and sedimentation including grain-size distribution (Flemings and Jordan, 1989; Simpson, 2006; Armitage et al., 2011). More complex models take into account the dynamics of three-dimensional landscapes incorporating full fluvial networks (Johnson and Beaumont, 1995; Garcia-Castellanos, 2002; Garcia-Castellanos et al. 2003,). Our approach aims to balance simplification of the system so that we can understand the main outputs of the model with approximating the first-order characteristics of the physical processes that govern the coupling in mountain range/foreland basin systems.

In order to investigate the coupling of topography and sediment flux during the evolution of a mountain range/foreland basin system, we use a modified version of a box-model introduced by Tucker and van der Beek (2013). We use this model to explore the relationship between crustal thickening, isostasy, topography and surface processes in the Pyrenees. The model analyses a single thrust wedge and foreland basin using two boxes that exchange mass with their surroundings by sediment transport, crustal thickening and tectonic accretion (Figure 5). Mass exchanges through the model follow two principles: i) mass conservation, which means that all material that exits a box has to be redistributed to its surroundings and ii) a correlation between topographic relief and sediment flux. The model is coupled with lithospheric flexural isostasy, which predicts the average deflection beneath the range and basin. Changes in the topographic elevation of the range (H_r) and basin (H_b) relative to a base level are then defined with the following equations:

$$\frac{dH_r}{dt} = (1 - \psi_r)\left(\frac{F_c + F_a - F_r}{\rho_r L_r}\right) \quad (1),$$

$$\frac{dH_b}{dt} = \frac{F_r - F_a - F_b}{\rho_b L_b} - \psi_b \frac{d\eta_r}{dt} \quad (2),$$

where F_c corresponds to accretionary flux of crustal rocks into the thrust wedge in response to plate convergence and underplating; F_a is the accretionary flux of basin sediments through frontal thrusting. F_r and F_b are respectively the sediment flux out of the range and sediment flux out of the basin; ρ_r and ρ_b are material density for the range and basin; L_r and L_b are the width of the range and basin perpendicular to their strike; η_r is the crustal thickness of the range and corresponds to $w_r + H_r$ where w_r the isostatic deflection depth of the range; and ψ_r and ψ_b are flexural isostatic parameters for the range and basin respectively.

The accretionary flux (F_c) is expressed with the following equation:

$$F_c = V_c T_c \rho_r \alpha \quad (3),$$

where V_c is the total convergence velocity, T_c is the thickness of the accreted rock. We introduce a new parameter α, which is not in the original model, where α is the proportion of the range formed by the pro- or retro-wedges (sensu Willett et al., 1993). Here, α is defined as L_r/L_t with L_t the total width of the range and L_r the width of the retro or pro-wedge. It implies that in the model, the length of the retro or pro-wedge is strictly defined by the position of the drainage divide (Figure 1B). This study focuses on the growth of the retro-wedge of the northern Pyrenees where the topography is dominated by crustal rocks (Figure 1C), and where the accretionary flux from the basin (F_a) is negligible in terms of the contribution to topography. If modelling a pro-wedge such as the southern Pyrenees, an additional accretionary flux term is needed to describe the incorporation of accreted basin sediments to the front of the wedge; this is the same as equation (3) but replaces ρ_r with ρ_b.

The sediment flux from the range to the basin (F_r) and the sediment flux from the foreland basin (F_b) to the outer depocentre (Figure 5) are defined as follow:

$$\frac{F_r}{\rho_r L_r} = \frac{1}{\tau_r}(H_r - H_b) \quad (4),$$

$$\frac{F_b}{\rho_b L_b} = \frac{1}{\tau_b} H_b \quad (5),$$

where τ_r and τ_b are the range and basin response times respectively and are defined as L^2/κ with L the width of the system and κ is the diffusive transport coefficient for the range or basin (Allen et al., 2008). We consider the ratio between the response times of the basin and the range to represent the relative efficiency of erosional processes between the basin and range. When the erosional response time ratio increases (i.e. the response time of the basin increases relative to the range), then the ability of the basin to transport sediment to an outer depocentre is less than that of the range to the basin, and so sediment will aggrade in the basin and the basin's elevation will increase.

The average deflection beneath the range (ψ_r) and basin (ψ_b) are given by the following equation (Watts, 2001):

$$\psi_r = \frac{\rho_r}{(\rho_m - \rho_b)} \frac{e^{-2\lambda L_r}\left(e^{2\lambda L_r}(-1 + 4\lambda L_r) + \cos(2\lambda L_r) - \sin(2\lambda L_r)\right)}{4\lambda L_r} \quad (6),$$

$$\psi_b = \frac{\rho_r}{2(\rho_m - \rho_b)} \frac{1}{3\pi - 4\lambda L_r} 2e^{-2\lambda L_r - 3\pi/4}\left(\sqrt{2}e^{\lambda L_r}\left(-1 + e^{2\lambda L_r}\right)\cos(\lambda L_r) + e^{3\pi/4}\left(e^{2\lambda L_r} - \cos(2\lambda L_r) + \sin(2\lambda L_r)\right)\right) \quad (7),$$

with ρ_m is mantle density and λ is the inverse flexural parameter. The inverse flexural parameter λ is related to the flexural rigidity D and lithosphere elastic thickness T_e, which corresponds to the rigidity of the lithosphere and the ability of the lithosphere to support the mass of the range.

4. Generic model sensitivity tests

We constructed a reference model with a simple history involving the growth, steady-state and decay of a retro-wedge/foreland basin system using general values for parameters derived from presently active mountain ranges (Batt et al., 1999). These values are V_c = 10 mm.yr^{-1}, T_c = 20 km, T_e = 22 km, α = 0.3, response time ratio of 0.33 and duration of convergence deceleration T of 2.5 Myr. Convergence is active from 60 to 30 Ma followed by a post-orogenic stage lasting 30 Myrs (i.e. 30 to 0 Ma). These experiments are aimed at understanding the controls on elevation change in the foreland basin relative to the mountain belt. The main result is that in all model runs, there is a predicted increase in the elevation of the basin during the initial post-orogenic stage. This unexpected signal, already observed in Tucker and van der Beek (2013), can be broadly assigned to continued high rates of sediment supply from the mountain range due to the high elevation contrast between the range and basin, combined with the cessation of basin subsidence and hence of creation of accommodation space to capture the sediment. Diminution of accommodation space should therefore lead to sediment aggradation in the basin and contribute to the increase in basin elevation. We focus on this response through a set of experiments that aim to evaluate the principle controls on this signal (Figure 6).

The model indicates that different parameters influence the post-orogenic response of the foreland basin (i.e. after 30 Ma). The convergence velocity (V_c) and the thickness of the accreted rock (T_c), which govern tectonic accretion in the range, have a similar impact (Figure 6A and B). This impact is enhanced by an increase in topographic response of the foreland basin following cessation of convergence with higher V_c and T_c. The observed trend is due to higher uplift rate and sediment flux toward the basin. The difference in the modelled increase in the post-orogenic elevation of the foreland basin is proportional to the maximum elevation achieved by the mountain range due to the changes of V_c or T_c. The lithosphere elastic thickness (T_e) corresponds to the rigidity of the lithosphere and the ability of the lithosphere to support the mass of the range. The relative proportion of the thrust-wedge width (α) compared with the full width of the range, directly determines the mass that loads the lithosphere and how much it will be flexed. These two parameters have therefore a similar effect on the foreland basin response. The main trend is a greater increase in elevation of the foreland basin after cessation of convergence at 30 Ma when T_e is lower or α is higher (Figure 6C and D). This effect is due to a greater flexural rebound after the cessation of convergence and therefore uplift of the basin after cessation of tectonics. Note that it takes longer for the system to reach steady-state during active convergence when T_e is lower or when α is higher. The inverse effect is also illustrated with a longer topographic elevation survival during the post-orogenic stage for both the range and the foreland basin when T_e is lower or when α is higher. The maximum elevation of the range at the end of the orogenic phase is also more important for an increase of the erosional response time ratio of the basin relative to the range, i.e. more sediment is delivered to the basin than can be removed (higher basin sedimentary influx than basin sedimentary outflux) (Figure 6E). Finally, the foreland basin shows different post-orogenic behaviour in response to varying the duration of convergence deceleration (T). When T increases, the basin elevation increase is lower, but elevation increases over a longer period (Figure 6F) as the isostatic rebound remains higher for a longer period of time.

In summary, the tendency for an increase in the elevation of the foreland basin relative to the range following the cessation of orogenesis is enhanced by: 1. Higher syn-orogenic convergence velocities; 2. Higher thickness of accreted material; 3. Lower lithosphere elastic thickness; 4. Higher proportion of range occupied by the retro-wedge; 5. A higher erosional response time ratio between the basin and the range; and 6. Shorter duration of convergence deceleration. We now apply the model to the northern Pyrenees using specific parameters and approximate the change in basin elevation of the

modelled Aquitaine Basin during the transition to post-orogenesis. We explore the implications of this evolution for post-orogenic topography and stratigraphy of the Aquitaine Basin.

5. Application to the Northern Pyrenees

5.1. Northern Pyrenean parameters

We apply the model to the north Pyrenean case study using parameter values constrained by the geological history since the onset of active convergence (see section 2). As the construction of orogenic topography in the Pyrenean system started around Paleocene times, we set the model to run over 66 Myrs simulating the full Cenozoic evolution. The main phase of convergence runs from 56 to 23 Ma, and mimics the main phase of topographic growth in the Pyrenees, followed by post-orogenic decay during Neogene and Quaternary time (i.e. 23 to 0 Ma) (Figure 7). Tectonic accretion is simulated using a plate convergence velocity of 3.2 mm.yr^{-1} from 56 to 41 Ma, 2.4 mm.yr^{-1} from 41 to 34 Ma, 4 mm.yr^{-1} from 34 to 23 Ma and 0.2 mm.yr^{-1} from 23 to 0 Ma (Macchiavelli et al., 2017) and a thickness of accreted crustal material of 30 km (Muñoz, 1992). The proportion of the retro-wedge relative to the total range width of 150 km is defined by an alpha factor of 0.3 based on the modern position of the drainage divide in the central Pyrenees (Figure 1B). The lithosphere elastic thickness can vary from 15 to 40 km (Angrand et al., 2018; Brunet, 1986; Curry et al., 2019; Desegaulx et al., 1990). The transport coefficient is selected from values ranging from 100 to 5,000 m^2.yr^{-1} for the range and from 1,000 to 50,000 m^2.yr^{-1} for the basin (Flemings and Jordan, 1989). Convergence deceleration starting at 23 Ma lasts from 2.5 to 7.5 Myrs.

5.2. Inverse modelling approach

The applicability of the model to the north Pyrenean study is strengthened by an inverse modelling search for the most probable set of parameter values in order to replicate first order geologic data of the northern Pyrenees (Figure 7). The robustness of the different outputs is assessed by comparing them with: i) a maximum mean elevation of the range during orogenesis of about 2 km, which has been independently quantified both by 3D flexural deformation and stratigraphic restoration (Curry et al., 2019) and by oxygen stable-isotope records and morphologic-hydrologic modelling studies (Huyghe et al., 2012); ii) the estimated depth of the Aquitaine foreland basin at 23 Ma of about 4.5 km (Ford et al., 2016); iii) the present-day mean elevations of the Pyrenees and Aquitaine foreland basin of about 1.5 km (Curry et al., 2019) and 0.25 km respectively. This approach allows us to obtain results that reproduce the main geometric features (i.e. range and basin topographic elevation and basin depth) of the Pyrenees (Figure 7).

In order to fully explore the parameter space during the inverse modelling search, a value is randomly chosen from a uniform distribution of the range of estimations of the controlling parameters (lithosphere elastic thickness, range transport coefficient, basin transport coefficient and convergence deceleration time). At each iteration, we calculate a root chi-square misfit function (χ) in order to measure the discrepancy between the observed (obs) data and the predicted (pre) results from the modified box-model:

$$\chi = \frac{1}{4}\sqrt{\frac{\left(H_{r,max}^{obs} - H_{r,max}^{pre}\right)^2}{{\delta H_{r,max}^{obs}}^2} + \frac{\left(H_{r,t0}^{obs} - H_{r,t0}^{pre}\right)^2}{{\delta H_{r,t0}^{obs}}^2} + \frac{\left(H_{b,t0}^{obs} - H_{b,t0}^{pre}\right)^2}{{\delta H_{b,t0}^{obs}}^2} + \frac{\left(w_{b,t23}^{obs} - w_{b,t23}^{pre}\right)^2}{{\delta w_{b,t23}^{obs}}^2}} \quad (8),$$

where $H_{r,max}$ is the maximum range elevation with uncertainty $\delta H_{r,max}$ = 0.2 km; $H_{r,t0}$ is the modern range elevation with uncertainty $\delta H_{r,t0}$ = 0.15 km; $H_{b,t0}$ is the modern basin elevation with uncertainty $\delta H_{b,t0}$ = 0.025 km and $w_{b,t0}$ is the basin depth at 23 Ma with uncertainty $\delta w_{b,t0}$ = 0.45 km.

5.3. Inverse modelling results

From the initial grid space exploration of 100 000 iterations, the model proposes ~500 solutions that converge towards a replication of the foreland basin depth, mean elevation of the range and basin and maximum elevation of the range with a misfit lower than 2 (Figure 8). The range of lithosphere elastic thickness in accepted models is 22.2±1.6 km. This value is in accordance with published lithosphere elastic thickness estimations for the northern Pyrenees. Brunet (1986) and Desegaulx et al., (1990) calculate a lithosphere elastic thickness of 21.93 km and 15 to 20 km. Angrand et al., (2018) propose a lithosphere elastic thickness of ~10 to ~25 km that increases away from the range. Finally, Curry et al., (2019) estimate a lithosphere elastic thickness of 23 km.

Model results predict diffusive transport coefficient of 430±140 $m^2.yr^{-1}$ and 13200±4400 $m^2.yr^{-1}$ for the range and the basin respectively. These values are in accordance with compiled transport coefficients from Flemings and Jordan (1989), which are of the order of 10^2-10^3 $m^2.yr^{-1}$ for the range and 10^4 $m^2.yr^{-1}$ for the basin.

The duration of the deceleration in convergence impacts the timing and amount of elevation change of the basin (Figure 6F). However, this parameter cannot be quantified for the northern Pyrenees with available geological data. Therefore, we retain the full range of proposed durations of convergence deceleration given by acceptable model solutions (i.e. 2.5 to 7.5 Myrs) (Supplementary Figure 1).

5.4. Modelled topography results

During the main Pyrenean orogenic phase (i.e. 56 to 23 Ma), the modelled range topography increases through time in proportion to the convergence velocity (Figure 9A). The elevation of the range reaches a maximum mean topography of 1980 m at the end of the syn-orogenic phase (23 Ma), which is comparable to the predicted maximum elevation of the range derived in other studies (see above). The post-orogenic phase (i.e. 23 to 0 Ma) results in an exponential decline in the mean elevation of the range to a mean value of 1400 m at the end of the model run. This value also approximates the present mean elevation of the Pyrenean range.

The elevation of the modelled foreland basin (Figure 9B) increases through time during the orogenic phase. Short periods of elevation decrease caused by the dominance of subsidence over sediment influx are recorded at the initiation of the higher convergence velocity phase (i.e. at 56 and 34 Ma). In contrast elevation increase is recorded at the onset of a phase of lower convergence velocity (i.e. 41 Ma). During the first stages of evolution of the modelled foreland basin, mean elevation of the basin remains negative meaning that it is underfilled. At ~42 Ma, elevation becomes positive and the basin becomes filled by sediment coming from the range. The basin is again briefly underfilled from 33 to 29 Ma due to acceleration in the convergent velocity. The transition to post-orogenesis in the modelled foreland basin is marked by an increase in mean elevation from ~85 to ~310 m followed by a general decrease to the end of the model run. The phase of increased elevation following cessation of convergence lasts up to ~8 Myrs (i.e. 23 to 15 Ma); this represents a period of basin elevation increase by isostatic rebound uplift and sediment aggradation. The mean elevation of the basin at the end of the model is ~240 m, which is comparable to the present day mean height of the Aquitaine Basin.

6. Discussion

6.1. Model predictions for the post-orogenic Aquitaine Basin

Topographic and sediment flux predictions in the box model used here are underpinned by a number of assumptions relating to the coupling of thrust wedge development and foreland basin sedimentation: (i) The first main assumption is the application of a rectangle box-model to a wedge-shape mountain range; this approach is considered a first-order approximation for the interaction of the

range and basin. The box-model is not intended to resolve localised deformation such as frontal accretion or internal thickening within a wedge, which generate higher frequency, punctuated surface process signals (e.g. Naylor and Sinclair, 2007) (ii) We assume a constant lithospheric elastic thickness for the European lithosphere. Studies have demonstrated however that lithosphere rigidity can vary through space (Angrand et al., 2018) and also through time (Curry et al., 2019). The generic model suggests this could impact the magnitude of the flexural rebound and therefore the elevation increase signal of the foreland basin during the post-orogenic phase. (iii) Variable erosion or deposition is not resolved by the model in either the range or foreland basin. Erosion rate and resulting sediment flux are defined by the elevation contrast between the mean height of the range and that of the basin. Whilst this does not reflect variations such as hillslope gradient, which assert an important control on erosion (Ahnert, 1970; Montgomery and Brandon, 2002) it could be seen as an approximation of channel steepness, which underpins the stream power model for fluvial incision (e.g. Tucker and Whipple, 2002). Similarly, variations in sediment grainsize are not accounted for here, but would affect the efficiency of sediment transport in the foreland basin (e.g. Duller et al., 2010). (iv) General evolutionary models coupling tectonics and surface processes indicate the development of a generally straight drainage divide roughly parallel with the mountain front and tracking the thickest part of a doubly-vergent wedge located above the S-point (Koons, 1990). The exact location of the drainage divide fluctuates around the S-point because of frontal accretion and underplating (Willet et al., 2001). The model approximates only the first order evolution of a thrust wedge/foreland basin system and therefore cannot address this natural variability.

Evolution of the foreland basin in the model is governed by three main processes: i) the flexure of the lithosphere, which can be negative when subsidence is active or positive during isostatic rebound, ii) the sedimentary influx from the range, which governs sediment accumulation of the foreland basin and iii) the sedimentary efflux from the basin to the outer basin, which simulates erosion and removal of material from the basin. During late syn-orogenesis, the majority of the sediment flux from the range is trapped in the foreland basin because of active lithospheric flexure (Figures 10A and 11A). Despite ongoing subsidence, foreland basin elevation increases because the sediment influx from the range to the basin is slightly greater than the accommodation space created by flexure (Figures 9B and 11A). However, tectonics and frontal thrust movements during active convergence should limit the formation of a sedimentary drape over the front of the range. During the early post-convergence phase (i.e. 23 to 20 Ma), the combination of reduced flexural subsidence, continued high sedimentary influx from the range and low basin outflux results in aggradation (Figure 10A) and hence an increased mean elevation of the foreland basin. Cessation of tectonic activity in the thrust wedge in combination with basin aggradation should allow sediments to drape and onlap the edge of the range (Figure 11B). From 23 Ma onwards, the topography of the range decays, causing an isostatic flexural rebound in both the range and the foreland basin (Figures 10A and 11C). Increase in the elevation of the foreland basin is now (i.e. ~20 to ~15 Ma) mainly due to the isostatic uplift component. The sediment outflux from the foreland basin to the outer basin becomes more important and counterbalances the influx of sediment into the basin, thus limiting aggradation and onlap onto the range (Figures 10 and 11C). From the onset of post-orogenesis (i.e. 23 Ma) to the maximum elevation of the foreland basin (i.e. ~15 Ma), the contribution of the sediment influx from the range to the basin is more important than the sediment outflux from the basin (Figure 8B). This phase of about 8 Myrs is mainly characterized by a decrease of range elevation and an increase of basin elevation (Figures 9AB and 10C). During the second part of the post-orogenic phase, sediment outflux from the foreland basin to the outer basin becomes more important than the sediment influx from the range, and this is associated with flexural rebound and uplift of the basin leading to net erosion (Figures 10 and 11D). Even if this last stage of erosion of the foreland basin is significant, evidence of sediment onlap onto the range from the early post-orogenic phase may be preserved as remnants on the mountain range (Figure 11D). This second phase from ~15 Ma to present-day is characterized by a reduction in elevation of both the range and foreland basin (Figures 9AB and 10C).

6.2. Topographic evolution and post-orogenic sediment drape in the Pyrenees

Topographic evolution of the Pyrenees during the Cenozoic period was recently modelled by Curry et al., (2019) through an inversion of the flexural subsidence of the foreland basins. They identify a limited decrease for the mean range elevation (i.e. ~1800 to ~1500 m) during the post-orogenic evolution, which is compatible with our results (Figure 9A). Our model results predict two main phases of topographic growth during Early Eocene and Early Oligocene times, controlled mainly by the convergence plate models of Macchiavelli et al., (2017). At contrary the main phase of topographic growth inferred by Curry et al., (2019) is limited to the Late Eocene based on the Aquitaine foreland basin record. A possible explanation for this main difference during Early Eocene is that we use a constant thickness of accreted material through time (i.e. 30 km). However, it is possible that the lithosphere thickness was lower during the Early Cenozoic limiting topographic growth during this period (Ford et al., 2016).

Our model predicts a maximum increase in mean elevation of about 220 m due to isostatic rebound and sediment aggradation above the previous height of the basin during the early post-orogenic stage (Figure 10C) with a maximum mean elevation of ~310 m (Figure 9B). If we assume a constant slope through the foreland basin from the front ranges to a distal pinchout that approximates sea-level, the mean elevation of ~310 m would correspond to a maximum elevation of ~620 m on the proximal part of the basin. With a basin width of about 120 km across the Aquitaine Basin, this would imply a mean fluvial gradient of ~0.32° across the basin, which is comparable to many modern fluvial gradients in similar settings (Blair and McPherson, 1994). This elevation range is in accordance with the maximum observed elevations of remnant modern Miocene sediment drapes in the Northern Pyrenees (i.e. ~600-700 m) (Figure 4).

The transient period during which the elevated foreland basin existed at the beginning of the post-orogenic stage (Figure 9B) in the model is in agreement with the geological age of the sediment cover observed on the Sub-Pyrenean Zone and North Pyrenean Zone. The model predicts an elevated basin from 23 to ~15 Ma, which corresponds to the Early and Middle Miocene age (Figure 2) of the sediment drape on the Northern Pyrenees (Figure 4). The age of the maximum elevation of the foreland basin as predicted by the model (~15 Ma) is a little older than the youngest sedimentation in the Northern Pyrenees foothills, which is estimated as Upper Serravallian (i.e. ~12 Ma). Recently, Ortiz et al., (2020) propose that generally the proximal part of the Aquitaine Basin during Early Miocene (i.e. ~23-15 Ma) was in by-pass and sedimentation occurred mainly in the distal part of the basin. Our model cannot spatially differentiate if sedimentation occurs in the proximal or distal part of the basin. However, there is evidences of Early and Middle Miocene sediments on the Sub-Pyrenean Zone and proximal part of the Aquitaine Platform which strengthen our model results and geological data correlation.

6.3. High elevation, low gradient surfaces and morphologic evolution of the Northern Pyrenees

Many of the locations that preserve sediment drapes are also characterised by low gradient surfaces in the landscape, which form an important feature of the Pyrenees on both sides of the range. It has been proposed that these surfaces result from planation near sea level and later uplift (Calvet and Gunnel, 2008; Gunnel et al., 2008) or that they originally formed at high elevation by the inhibition of erosion because of piedmont sedimentation (Mellere, 1993; Coney et al., 1996; Babault et al., 2005a). The latter has been demonstrated for the southern Pyrenees where thick continental deposits filled the Ebro foreland basin (Babault et al., 2005a) and reached elevations up to ~1700 m in the Southern Pyrenean Thrust Belt. However, comparably high signals are ambiguous in the northern Pyrenees. Elevation increase by post-orogenic sediment aggradation from our modelling results suggests a maximum mean elevation of ~300 m above the deformation front (Fig. 9B) meaning an elevation of about 600 m at the Pyrenean range front. Projection of this surface into the range can explain the

presence of low-gradient surfaces in the northern Pyrenees, which are generally at lower elevations compared to the southern Pyrenees (Bosch et al., 2016).

The topographic survival of post-orogenic mountain ranges has been an enigmatic problem (Baldwin et al., 2003). The Pyrenees still preserve high topography despite cessation of major convergence at the beginning of Miocene times (i.e. ~23 Ma; Muñoz et al., 1992; Beaumont et al., 2000). Early research predicted a short period of topographic survival in a mountainous area by dividing the mean elevation of mountain ranges by the average denudation rate (Gilluly, 1955). Simple models of landscape evolution demonstrate an exponential decay of mountain topography (Stephenson, 1984; Tucker and van der Beek, 2013). Several factors can inhibit post-orogenic topographic decay such as resistant lithologies, isostatic response of the lithosphere and controls on fluvial erosion (Baldwin et al., 2003). One of the most important aspects of fluvial erosion in the persistence of topography is the relative roles for detachment-limited (i.e. bedrock) versus transport-limited (i.e. alluvial) river conditions. Numerical landscape evolution models incorporating both detachment and transport-limited conditions predict a transition to the transport-limited condition during post-orogenesis (Whipple and Tucker, 2002; Baldwin et al., 2013) and an increase in decay times. Our results support this hypothesis where alluvial aggradation during the post-orogenic period inhibits channel erosion and allows for a longer persistence of mountain topography.

The current model cannot resolve fluvial transport and erosion, but the combination of low range transport coefficients and low lithosphere elastic thickness predicted by the inverse modelling (Fig. 8) allow us to simulate limited topographic decay for the northern Pyrenees (Figure 9A) as proposed by Babault et al., (2005a) and Curry et al., (2019). Low values for the range transport coefficient limit erosion in the range and coupled with a low lithosphere elastic thickness imply an important isostatic effect to maintain topography in the thrust wedge through time. Relatively stable topography in the range is also maintained during the post-orogenic stage because of the elevated foreland basin (Figures 9B and 10), which reduces relief and inhibits erosion (Figure 9C) as demonstrated in Babault et al., (2005a).

6.4. Evidence from other mountain belt-foreland basin systems

The North Alpine Foreland Basin (NAFB) of the European Alps records deposition from Maastrichtian to middle Miocene. Sedimentation in the NAFB can be summarized by an early deep-water stage with deposition of the Ultrahelvetic flysch and North Helvetic flysch (Allen et al., 1991) followed by shallow-marine/continental flysch and molasse (Allen et al., 1991). First-order behaviour of the basin is characterized by an underfilled basin before mid-Oligocene time following by an overfilled basin (Sinclair and Allen, 1992). In Late Miocene, the basin switched from deposition to erosion as tectonic activity ceased because of isostatic rebound (Cederbom et al., 2004). The NAFB does not seem to record an overfilled trend but rather an erosive unconformity during the transition. The extent to which any deposits younger than the preserved uppermost Upper Freshwater Molasse (ca. 11 Ma; Bolliger, 1998) draped the outer margins of the thrust belt is unclear due principally to poor preservation. The NAFB and northern European Alps are a pro-wedge system with relatively higher convergence rate compare to the Pyrenean system. Isostatic rebound at the post-orogenic transition, also enhanced by a wetter climate change (Cederbom et al., 2004) and resulting unroofing erosion of the NAFB, may have been too high to preserve a deposition signal during the early post-orogenic phase. This suggest that the preservation of early post-orogenic sediments in foreland basins can be quite rare and requires relatively stable conditions without major external forces changes.

Although the NAFB does not preserved early post-orogenic sediments, an increase of sediment flux out of the system is recorded in surrounding depositional settings (i.e. Rhône Delta, Rhône Graben and North Sea; Kuhlemann, 2000). This pattern is in agreement with our results, which indicate important erosional efflux out of the basin after cessation of tectonics (Figure 9D). Similar pattern is recorded for the Northern Pyrenees with an increase of sediment accumulation in the deep-sea plain of the margin (i.e. Bay of Biscay) during the post-orogenic period (Ortiz et al., 2020).

7. Conclusions

1. Topographic and geologic data from the northern Pyrenees characterise a post-orogenic sediment drape on the northern thrust wedge that corresponds to the deposition of large alluvial fans. Sediment drapes form low gradient-high elevation surfaces that range in elevation from ~300 to 600 m.

2. Experiments using a box model which approximate dynamic coupling of a thrust wedge/foreland basin system indicate that at the transition from syn-orogenesis to post-orogenesis, sediment flux from the range remains high, while basin subsidence slows; this combination results in accumulation of continental sediment that can drape over the frontal portions of thrust wedges.

3. By deriving a set of parameter values that approximate the north Pyrenean thrust belt and Aquitaine Basin system, we propose a mechanism of early post-orogenic aggradation to explain the deposition of middle Miocene conglomerates that drape the Sub-Pyrenean zone and North Pyrenean Thrust Belt. The model suggests that this aggradation of the Aquitaine Basin continued to an elevation of ~620 m on the proximal part of the foreland basin and lasted ~8 Ma following the onset of post-orogenesis (i.e. 23 to ~15 Ma). Miocene sediments that drape and seal tectonic structures of the Sub-Pyrenean Thrust and North Pyrenean Frontal Thrust are found at high elevations up to 600-700 m. Our modelling results indicate that these features are explained without evoking external forcing such as trapping of sediment or climate change.

4. Inverse modelling results explain the persistence of Pyrenean topography long after cessation of orogenic activity by low lithosphere elastic thickness and low range transport coefficient parameters and a reduction of relief between the range and basin.

Author contributions

All authors, T.B., H.D.S., M.N., F.C. and M.F., contributed to the writing of the text. T.B. and M.N designed and performed the numerical modelling. T.B., F.C. and H.D.S. explored post-orogenic field data from the Northern Pyrenees. M.F. and H.D.S. initiated the project.

References

Ahnert, F. (1970). Functional relationships between denudation, relief, and uplift in large, mid-latitude drainage basins. *American Journal of Science*. https://doi.org/10.2475/ajs.268.3.243

Allen, P. A., Homewood, P., & Williams, G. D. (1986). Foreland basins: an introduction. In Foreland basins. *Inter. Assoc. Sediment., Spec. Pub.* Vol. 8, pp. 3-12.

Allen, P. A. (2008). Time scales of tectonic landscapes and their sediment routing systems. *Geological Society, London, Special Publications*. https://doi.org/10.1144/sp296.2

Allen, P. A., Crampton, S. L., & Sinclair, H. D. (1991). The inception and early evolution of the north Alpine foreland basin, Switzerland. *Basin Research*. https://doi.org/10.1111/j.1365-2117.1991.tb00124.x

Allen, P. A., & Allen, J. R. (2005). *Basin Analyses, Principles and Applications*. Blackwell Oxford.

Angrand, P., Ford, M., & Watts, A. B. (2018). Lateral Variations in Foreland Flexure of a Rifted Continental Margin: The Aquitaine Basin (SW France). Tectonics. https://doi.org/10.1002/2017TC004670

Armitage, J. J., Duller, R. A., Whittaker, A. C., & Allen, P. A. (2011). Transformation of tectonic and climatic signals from source to sedimentary archive. Nature Geoscience. https://doi.org/10.1038/ngeo1087

Babault, J., Van Den Driessche, J., Bonnet, S., Castelltort, S., & Crave, A. (2005a). Origin of the highly elevated Pyrenean peneplain. *Tectonics*. https://doi.org/10.1029/2004TC001697

Babault, J., Bonnet, S., Crave, A., & Van Den Driessche, J. (2005b). Influence of piedmont sedimentation on erosion dynamics of an uplifting landscape: An experimental approach. Geology. https://doi.org/10.1130/G21095.1

Babault, J., Bonnet, S., Driessche, J. Van Den, & Crave, A. (2007). High elevation of low-relief surfaces in mountain belts: Does it equate to post-orogenic surface uplift? Terra Nova. https://doi.org/10.1111/j.1365-3121.2007.00746.x

Baldwin, J. A., Whipple, K. X., & Tucker, G. E. (2003). Implications of the shear stress river incision model for the timescale of postorogenic decay of topography. *Journal of Geophysical Research: Solid Earth*. https://doi.org/10.1029/2001JB000550

Barrouquère, G., Roux, L., Souquet, P., Peybernes, B., Rey, J., Debroas, E. J., Lagasquie, J., Ternet, Y., Bois, J. P., & Bambier, J. P. (1976). Carte géol. France (1/50000), feuille ST-GIRONS (1074). *Orléans: Bureaux de recherches géologiques et minières.*

Batt, G. E., & Braun, J. (1999). The tectonic evolution of the Southern Alps, New Zealand: Insights from fully thermally coupled dynamical modelling. Geophysical Journal International. https://doi.org/10.1046/j.1365-246X.1999.00730.x

Beaumont, C. (1981). Foreland basins. *Geophysical Journal of the Royal Astronomical Society*. https://doi.org/10.1111/j.1365-246X.1981.tb02715.x

Beaumont, C., Muñoz, J. A., Hamilton, J., & Fullsack, P. (2000). Factors controlling the Alpine evolution of the central Pyrenees inferred from a comparison of observations and geodynamical models. *Journal of Geophysical Research: Solid Earth*. https://doi.org/10.1029/1999JB900390

Bernard, T., Sinclair, H. D., Gailleton, B., Mudd, S. M., & Ford, M. (2019). Lithological control on the post-orogenic topography and erosion history of the Pyrenees. *Earth and Planetary Science Letters*. https://doi.org/10.1016/j.epsl.2019.04.034

Biteau, J.-J., Le Marrec, A., Le Vot, M., & Masset, J.-M. (2006). The Aquitaine Basin. *Petroleum Geoscience*. https://doi.org/10.1144/1354-079305-674

Blair, T. C., & McPherson, J. G. (1994). Alluvial fans and their natural distinction from rivers based on morphology, hydraulic processes, sedimentary processes, and facies assemblages. *Journal of Sedimentary Research A: Sedimentary Petrology & Processes.* https://doi.org/10.1306/d42681b2-2b26-11d7-8648000102c1865d

Bolliger T. H. (1998). Age and geographic distribution of the youngest Upper Freshwater Molasse (OSM) of eastern Switzerland. *Eclogae Geologicae Helvetiae*. V.91(3), p. 321-332.

Bosch, G. V., Van Den Driessche, J., Babault, J., Robert, A., Carballo, A., Le Carlier, C., … Baudin, T. (2016). Peneplanation and lithosphere dynamics in the Pyrenees. *Comptes Rendus - Geoscience*. https://doi.org/10.1016/j.crte.2015.08.005

Bourrouilh, R., Richert, J. P., & Zolnai, G. (1995). The north Pyrenean Aquitaine Basin, France: evolution and hydrocarbons. American Association of Petroleum Geologists Bulletin. https://doi.org/10.1306/8d2b1bc4-171e-11d7-8645000102c1865d

Braun, J., Van Der Beek, P., & Batt, G. (2006). *Quantitative thermochronology: Numerical methods for the interpretation of thermochronological data*. *Quantitative Thermochronology: Numerical Methods for the Interpretation of Thermochronological Data*. https://doi.org/10.1017/CBO9780511616433

Brunet, M. F. (1986). The influence of the evolution of the Pyrenees on adjacent basins. *Tectonophysics*. https://doi.org/10.1016/0040-1951(86)90260-X

Burbank, D. W. (1992). Causes of recent Himalayan uplift deduced from deposited patterns in the Ganges basin. *Nature*. https://doi.org/10.1038/357680a0

Calvet, M., & Gunnell, Y. (2008). Planar landforms as markers of denudation chronology: an inversion of East Pyrenean tectonics based on landscape and sedimentary basin analysis. *Geological Society, London, Special Publications*. https://doi.org/10.1144/SP296.10

Carretier, S., & Lucazeaut, F. (2005). How does alluvial sedimentation at range fronts modify the erosional dynamics of mountain catchments? Basin Research. https://doi.org/10.1111/j.1365-2117.2005.00270.x

Cederbom, C. E., Sinclair, H. D., Schlunegger, F., & Rahn, M. K. (2004). Climate-induced rebound and exhumation of the European Alps. *Geology*. https://doi.org/10.1130/G20491.1

Cederbom, C. E., Van Der Beek, P., Schlunegger, F., Sinclair, H. D., & Oncken, O. (2011). Rapid extensive erosion of the North Alpine foreland basin at 5-4Ma. Basin Research. https://doi.org/10.1111/j.1365-2117.2011.00501.x

Champagnac, J. D., Molnar, P., Anderson, R. S., Sue, C., & Delacou, B. (2007). Quaternary erosion-induced isostatic rebound in the western Alps. *Geology*. https://doi.org/10.1130/G23053A.1

Champagnac, J. D., Schlunegger, F., Norton, K., von Blanckenburg, F., Abbühl, L. M., & Schwab, M. (2009). Erosion-driven uplift of the modern Central Alps. Tectonophysics. https://doi.org/10.1016/j.tecto.2009.02.024

Coney, P. J., Muñoz, J. A., McClay, K. R., & Evenchick, C. A. (1996). Syntectonic burial and post-tectonic exhumation of the southern Pyrenees foreland fold-thrust belt. *Journal of the Geological Society*. https://doi.org/10.1144/gsjgs.153.1.0009

Curry, M. E., van der Beek, P., Huismans, R. S., Wolf, S. G., & Muñoz, J. A. (2019). Evolving paleotopography and lithospheric flexure of the Pyrenean Orogen from 3D flexural modeling and basin analysis. *Earth and Planetary Science Letters*. https://doi.org/10.1016/j.epsl.2019.03.009

Debroas, E. J. (1990). Le Flysch noir albo-cenomanien temoin de la structuration albienne a senonienne de la Zone nord-pyreneenne en Bigorre (Hautes-Pyrenees, France). Bulletin - Societe Geologique de France. https://doi.org/10.2113/gssgfbull.vi.2.273

Desegaulx, P., Roure, F., & Villein, A. (1990). Structural evolution of the Pyrenees: tectonic inheritance and flexural behaviour in the continental crust. *Tectonophysics*. https://doi.org/10.1016/0040-1951(90)90164-4

Dickinson, W. R., (1974). Plate tectonics and sedimentation. In *Tectonics and sedimentation: SEPM Special Publication*.

Duller, R. A., Whittaker, A. C., Fedele, J. J., Whitchurch, A. L., Springett, J., Smithells, R., … Allen, P. A. (2010). From grain size to tectonics. Journal of Geophysical Research: Earth Surface. https://doi.org/10.1029/2009JF001495

Fillon, C., Gautheron, C., & van der Beek, P. (2013). Oligocene–Miocene burial and exhumation of the Southern Pyrenean foreland quantified by low-temperature thermochronology. *Journal of the Geological Society*. https://doi.org/10.1144/jgs2012-051

Fitzgerald, P. G., Muñoz, J. A., Coney, P. J., & Baldwin, S. L. (1999). Asymmetric exhumation across the Pyrenean orogen: Implications for the tectonic evolution of a collisional orogen. *Earth and Planetary Science Letters*. https://doi.org/10.1016/S0012-821X(99)00225-3

Flemings, P. B., & Jordan, T. E. (1989). A synthetic stratigraphic model of foreland basin development. *Journal of Geophysical Research*. https://doi.org/10.1029/JB094iB04p03851

Ford, M., Hemmer, L., Vacherat, A., Gallagher, K., & Christophoul, F. (2016). Retro-wedge foreland basin evolution along the ECORS line, eastern Pyrenees, France. *Journal of the Geological Society*. https://doi.org/10.1144/jgs2015-129

Garcia-Castellanos, D. (2002). Interplay between lithospheric flexure and river transport in foreland basins. Basin Research. https://doi.org/10.1046/j.1365-2117.2002.00174.x

Garcia-Castellanos, D., Vergés, J., Gaspar-Escribano, J., & Cloetingh, S. (2003). Interplay between tectonics, climate, and fluvial transport during the Cenozoic evolution of the Ebro Basin (NE Iberia). *Journal of Geophysical Research: Solid Earth*. https://doi.org/10.1029/2002JB002073

Garver, J. I., Brandon, M. T., Roden-Tice, M., & Kamp, P. J. J. (1999). Exhumation history of orogenic highlands determined by detrital fission-track thermochronology. *Geological Society, London, Special Publications*. https://doi.org/10.1144/gsl.sp.1999.154.01.13

Gibson, M., Sinclair, H. D., Lynn, G. J., & Stuart, F. M. (2007). Late- to post-orogenic exhumation of the central Pyrenees revealed through combined thermochronological data and modelling. *Basin Research*. https://doi.org/10.1111/j.1365-2117.2007.00333.x

Gilluly, J., (1955). Geologic contrasts between continents and ocean basins. *GeoL Soc. Amer*.

Grool, A. R., Ford, M., Vergés, J., Huismans, R. S., Christophoul, F., & Dielforder, A. (2018). Insights Into the Crustal-Scale Dynamics of a Doubly Vergent Orogen From a Quantitative Analysis of Its Forelands: A Case Study of the Eastern Pyrenees. Tectonics. https://doi.org/10.1002/2017TC004731

Gunnell, Y., Zeyen, H., & Calvet, M. (2008). Geophysical evidence of a missing lithospheric root beneath the Eastern Pyrenees: Consequences for post-orogenic uplift and associated geomorphic signatures. *Earth and Planetary Science Letters*. https://doi.org/10.1016/j.epsl.2008.09.031

Heller, P. L., Angevine, C. L., Winslow, N. S., & Paola, C. (1988). Two-phase stratigraphic model of foreland-basin sequences. *Geology*. https://doi.org/10.1130/0091-7613(1988)016<0501:TPSMOF>2.3.CO;2

Homewood, P., Allen, P. A., & Williams, G. D. (1986). Dynamics of the Molasse Basin of western Switzerland. Foreland Basins. https://doi.org/10.1002/9781444303810.ch10

Huyghe, D., Mouthereau, F., & Emmanuel, L. (2012). Oxygen isotopes of marine mollusc shells record Eocene elevation change in the Pyrenees. Earth and Planetary Science Letters. https://doi.org/10.1016/j.epsl.2012.06.035

Johnson, D. D., & Beamont, C. (1995). Preliminary results from a planform kinematic model of orogen evolution, surface processes and the development of clastic foreland basin stratigraphy. In *Stratigraphic Evolution of Foreland Basins*. https://doi.org/10.2110/pec.95.52.0003

Jolivet, L., Gorini, C., Smit, J., & Leroy, S. (2015). Continental breakup and the dynamics of rifting in back-arc basins: The Gulf of Lion margin. *Tectonics*. https://doi.org/10.1002/2014TC003570

Jolivet, M., Labaume, P., Monié, P., Brunel, M., Arnaud, N., & Campani, M. (2007). Thermochronology constraints for the propagation sequence of the south Pyrenean basement thrust system (France-Spain). *Tectonics*. https://doi.org/10.1029/2006TC002080

Jordan, T. E. (1981). Thrust loads and foreland basin evolution, Cretaceous, western United States. *AAPG Bulletin*. https://doi.org/10.1306/03B599F4-16D1-11D7-8645000102C1865D

Koons, P. O. (1990). Two-sided orogen: collision and erosion from the sandbox to the Southern Alps, New Zealand. Geology. https://doi.org/10.1130/0091-7613(1990)018<0679:TSOCAE>2.3.CO;2

Kuhlemann, A. (2000). Post-collisional sediment budget of circum-Alpine basins (central Europe). *Padova, Estratto da Memorie di Scienze Geologiche*.

Macchiavelli, C., Vergés, J., Schettino, A., Fernàndez, M., Turco, E., Casciello, E., … Tunini, L. (2017). A New Southern North Atlantic Isochron Map: Insights Into the Drift of the Iberian Plate Since the Late Cretaceous. *Journal of Geophysical Research: Solid Earth*. https://doi.org/10.1002/2017JB014769

Mellere, D. (1993). Thrust-Generated, Back-Fill Stacking of Alluvial Fan Sequences, South-Central Pyrenees, Spain (La Pobla De Segur Conglomerates). In *Tectonic Controls and Signatures in Sedimentary Successions*. https://doi.org/10.1002/9781444304053.ch14

Metcalf, J. R., Fitzgerald, P. G., Baldwin, S. L., & Muñoz, J. A. (2009). Thermochronology of a convergent orogen: Constraints on the timing of thrust faulting and subsequent exhumation of the Maladeta Pluton in the Central Pyrenean Axial Zone. *Earth and Planetary Science Letters*. https://doi.org/10.1016/j.epsl.2009.08.036

Monod, B., Bourroullec, I., Chèvremont, P., LeBayon, B., Nehlig, P., Aretz, M., Bilotte, M., Christophoul, F., Debroas, E.-J., Denèle, Y., Faure, M., Laumonier, B., Lézin, C., Nardin, E., Olivier, P., Regard, V., de St Blanquat, M. (2014) *Carte géologique numérique à 1/250 000 de la région Midi-Pyrénées, Notice*.

Montgomery, D. R., & Brandon, M. T. (2002). Topographic controls on erosion rates in tectonically active mountain ranges. *Earth and Planetary Science Letters*. https://doi.org/10.1016/S0012-821X(02)00725-2

Morris, R. G., Sinclair, H. D., & Yelland, A. J. (1998). Exhumation of the Pyrenean Orogen: implications for sediment discharge. *Basin Research*. https://doi.org/10.1046/j.1365-2117.1998.00053.x

Mouchené, M., van der Beek, P., Mouthereau, F., & Carcaillet, J. (2017). Controls on Quaternary incision of the Northern Pyrenean foreland: Chronological and geomorphological constraints from the Lannemezan megafan, SW France. *Geomorphology*. https://doi.org/10.1016/j.geomorph.2016.12.027

Mouthereau, F., Filleaudeau, P. Y., Vacherat, A., Pik, R., Lacombe, O., Fellin, M. G., … Masini, E. (2014). Placing limits to shortening evolution in the Pyrenees: Role of margin architecture and implications for the Iberia/Europe convergence. *Tectonics*. https://doi.org/10.1002/2014TC003663

Muñoz, J. A. (1992). Evolution of a continental collision belt: ECORS-Pyrenees crustal balanced cross-section. In *Thrust Tectonics*. https://doi.org/10.1007/978-94-011-3066-0_21

Naylor, M., & Sinclair, H. D. (2008). Pro- vs. retro-foreland basins. *Basin Research*. https://doi.org/10.1111/j.1365-2117.2008.00366.x

Olivet, J. L. (1996). La cinématique de la plaque ibérique. *Bull. Cent. Rech. Explor. Prod. Elf Aquitaine*.

Ortiz, A., Guillocheau, F., Lasseur, E., Briais, J., Robin, C., Serrano, O., Fillon, C. (2020) Sediment routing system and sink preservation during post-orogenic evolution of a retro-foreland basin : The case example of the North Pyrenean (Aquitaine, Bay of Biscay) Basins. *Marine and Petroleum Geology*. https://doi.org/10.1016/j.marpetgeo.2019.104085

Paris, J. P., Icole, M., Tegyey, A., Monciardini, C., Andreieff, P., & Collignon, M. (1975) Carte géol. France (1/50000), feuille MONTREJEAU (1054). *Orléans: Bureaux de recherches géologiques et minières.*

Paris, J. P., & Monciardini, C. (1971). Carte géol. France (1/50000), feuille ST-GAUDENS. *Orléans: Bureaux de recherches géologiques et minières.*

Pelletier, J. D. (2004). The influence of piedmont deposition on the time scale of mountain-belt denudation. Geophysical Research Letters. https://doi.org/10.1029/2004GL020052

Pfiffner, O. A. (2009). Evolution of the North Alpine Foreland Basin in the Central Alps. In *Foreland Basins*. https://doi.org/10.1002/9781444303810.ch11

Reiners, P. W., Campbell, I. H., Nicolescu, S., Allen, C. M., Hourigan, J. K., Garver, J. I., … Cowan, D. S. (2005). (U-Th)/(He-Pb) double dating of detrital zircons. *American Journal of Science*. https://doi.org/10.2475/ajs.305.4.259

Roest, W. R., & Srivastava, S. P. (1991). Kinematics of the plate boundaries between Eurasia, Iberia, and Africa in the North Atlantic from the Late Cretaceous to the present. *Geology*. https://doi.org/10.1130/0091-7613(1991)019<0613:KOTPBB>2.3.CO;2

Rosenbaum, G., Lister, G. S., & Duboz, C. (2002). Relative motions of Africa, Iberia and Europe during Alpine orogeny. *Tectonophysics*. https://doi.org/10.1016/S0040-1951(02)00442-0

Rougier, G., Ford, M., Christophoul, F., & Bader, A. G. (2016). Stratigraphic and tectonic studies in the central Aquitaine Basin, northern Pyrenees: Constraints on the subsidence and deformation history of a retro-foreland basin. *Comptes Rendus - Geoscience*. https://doi.org/10.1016/j.crte.2015.12.005

Roure, F., Choukroune, P., Berastegui, X., Muñoz, J. A., Villien, A., Matheron, P., … Deramond, J. (1989). Ecors deep seismic data and balanced cross sections: Geometric constraints on the evolution of the Pyrenees. *Tectonics*. https://doi.org/10.1029/TC008i001p00041

Sanyal, P., Bhattacharya, S. K., Kumar, R., Ghosh, S. K., & Sangode, S. J. (2004). Mio-Pliocene monsoonal record from Himalayan foreland basin (Indian Siwalik) and its relation to vegetational change. *Palaeogeography, Palaeoclimatology, Palaeoecology*. https://doi.org/10.1016/j.palaeo.2003.11.013

Seguret, M. (1972). Étude tectonique des nappes et séries décollées de la partie centrale du versant sud des Pyrénées. *Pub. Estela, Ser geol. struct*.

Serrano, O., Delmas, J., Hanot, F., Vially, R., Herbin, J. P., Houel, P., & Tourlière, B. (2006). Le bassin d'Aquitaine: Valorisation des données sismiques, cartographie structurale et potentiel pétrolier, *Rapport Régional d'Evaluation Pétrolière. Bureau de la Recherche Géologique et Minière, Orléans, France, 245*.

Sibuet, J. C., Srivastava, S. P., & Spakman, W. (2004). Pyrenean orogeny and plate kinematics. Journal of Geophysical Research: Solid Earth. https://doi.org/10.1029/2003JB002514

Simpson, G. D. H. (2006). Modelling interactions between fold-thrust belt deformation, foreland flexure and surface mass transport. Basin Research. https://doi.org/10.1111/j.1365-2117.2006.00287.x

Sinclair, H. D., & Allen, P. A. (1992). Vertical versus horizontal motions in the Alpine orogenic wedge: Stratigraphic response in the foreland basin. *Basin Research*. https://doi.org/10.1111/j.1365-2117.1992.tb00046.x

Sinclair, H. D., Coakley, B. J., Allen, P. A., & Watts, A. B. (1991). Simulation of Foreland Basin Stratigraphy using a diffusion model of mountain belt uplift and erosion: An example from the central Alps, Switzerland. Tectonics. https://doi.org/10.1029/90TC02507

Sinclair, H. (2012). Thrust Wedge/Foreland Basin Systems. In Tectonics of Sedimentary Basins: Recent Advances. https://doi.org/10.1002/9781444347166.ch26

Sinclair, H. D., & Naylor, M. (2012). Foreland basin subsidence driven by topographic growth versus plate subduction. *Bulletin of the Geological Society of America*. https://doi.org/10.1130/B30383.1

Sinclair, H. D., Gibson, M., Naylor, M., & Morris, R. G. (2005). Asymmetric growth of the Pyrenees revealed through measurement and modeling of orogenic fluxes. *American Journal of Science*. https://doi.org/10.2475/ajs.305.5.369Souquet, P., Rey, J., Peybernès, B., Bilotte, M., Cosson, J., Cavaillé, A., Roche, J. H., & Bambier, A. (1977). Carte géol. France (1/50000), feuille LE MAS-D'AZIL (1056). Orléans: Bureaux de recherches géologiques et minières.

Stephenson, R. (1984). Flexural models of continental lithosphere based on the long-term erosional decay of topography. *Geophysical Journal of the Royal Astronomical Society*. https://doi.org/10.1111/j.1365-246X.1984.tb01940.x

Ternet, Y., Crouzel, F., Mirabail, H., Rey, E., Bouvier, A., Mediavilla, F., Debroas, E. J., Gatinot, F. (1988). Carte géol. France (1/50000), feuille BAGNÈRES-DE-BIGORRE (1053). *Orléans: Bureaux de recherches géologiques et minières.*

Tucker, G. E., & Whipple, K. X. (2002). Topographic outcomes predicted by stream erosion models: Sensitivity analysis and intermodel comparison. Journal of Geophysical Research: Solid Earth. https://doi.org/10.1029/2001jb000162

Tucker, G. E., & van der Beek, P. (2013). A model for post-orogenic development of a mountain range and its foreland. *Basin Research*. https://doi.org/10.1111/j.1365-2117.2012.00559.x

Vacherat, A., Mouthereau, F., Pik, R., Bellahsen, N., Gautheron, C., Bernet, M., … Radal, J. (2016). Rift-to-collision transition recorded by tectonothermal evolution of the northern Pyrenees. *Tectonics*. https://doi.org/10.1002/2015TC004016

Verges, J., & Muñoz, J. A. (1990). Thrust sequences in the southern central {Pyrenees}. Bulletin de La Société Géologique de France. https://doi.org/10.2113/gssgfbull.VI.2.265

Vergés, J., Fernàndez, M., & Martìnez, A. (2002). The Pyrenean orogen: Pre-, syn-, and post-collisional evolution. *Journal of the Virtual Explorer*. https://doi.org/10.3809/jvirtex.2002.00058

Vissers, R. L. M., & Meijer, P. T. (2012). Iberian plate kinematics and Alpine collision in the Pyrenees. *Earth-Science Reviews*. https://doi.org/10.1016/j.earscirev.2012.05.001

Watts, A. B. (2001). Isostasy and Flexure of the Lithosphere. *Cambridge University Press*.

Willett, S., Beaumont, C., & Fullsack, P. (1993). Mechanical model for the tectonics of doubly vergent compressional orogens. Geology. https://doi.org/10.1130/0091-7613(1993)021<0371:MMFTTO>2.3.CO;2

Willett, S. D., Slingerland, R., & Hovius, N. (2001). Uplift, shortening, and steady state topography in active mountain belts. *American Journal of Science*. https://doi.org/10.2475/ajs.301.4-5.455

Xie, X., & Heller, P. L. (2009). Plate tectonics and basin subsidence history. *Bulletin of the Geological Society of America*. https://doi.org/10.1130/B26398.1

Yelland, A. J. (1990). Fission track thermotectonics in the Pyrenean orogen. *International Journal of Radiation Applications and Instrumentation. Part*. https://doi.org/10.1016/1359-0189(90)90049-4

Tables

TABLE1: MODEL PARAMETERS

Parameter	Symbol	Value
Crustal rock density	ρ_r	2700 kg.m^{-3}
Mantle density	ρ_m	3300 kg.m^{-3}
Basin sediment density	ρ_b	1620 kg.m^{-3}
Effective elastic thickness	T_e	15,000 - 40,000 m
Young's modulus	E	1 x 10^{11} Pa
Poisson's ration	v	0.25
Gravity density	g	9.81 N.kg^{-1}
Range width	L_t	150,000 m
Alpha	α	0.3
Convergence velocity	V_c	0.0024 m.yr^{-1}
		0.0032 m.yr^{-1}
		0.004 m.yr^{-1}
		0.0002 m.yr^{-1}
Convergence tickness	T_c	30,000 m
Range transport coefficient	κ_r	100 - 5000 m^2.yr^{-1}
Basin transport coefficient	κ_b	1,000 - 50,000 m^2.yr^{-1}
Duration time		66 x 10^6 yrs
Iterations		100,000

Table 1. Input parameters for numerical modelling.

Figures

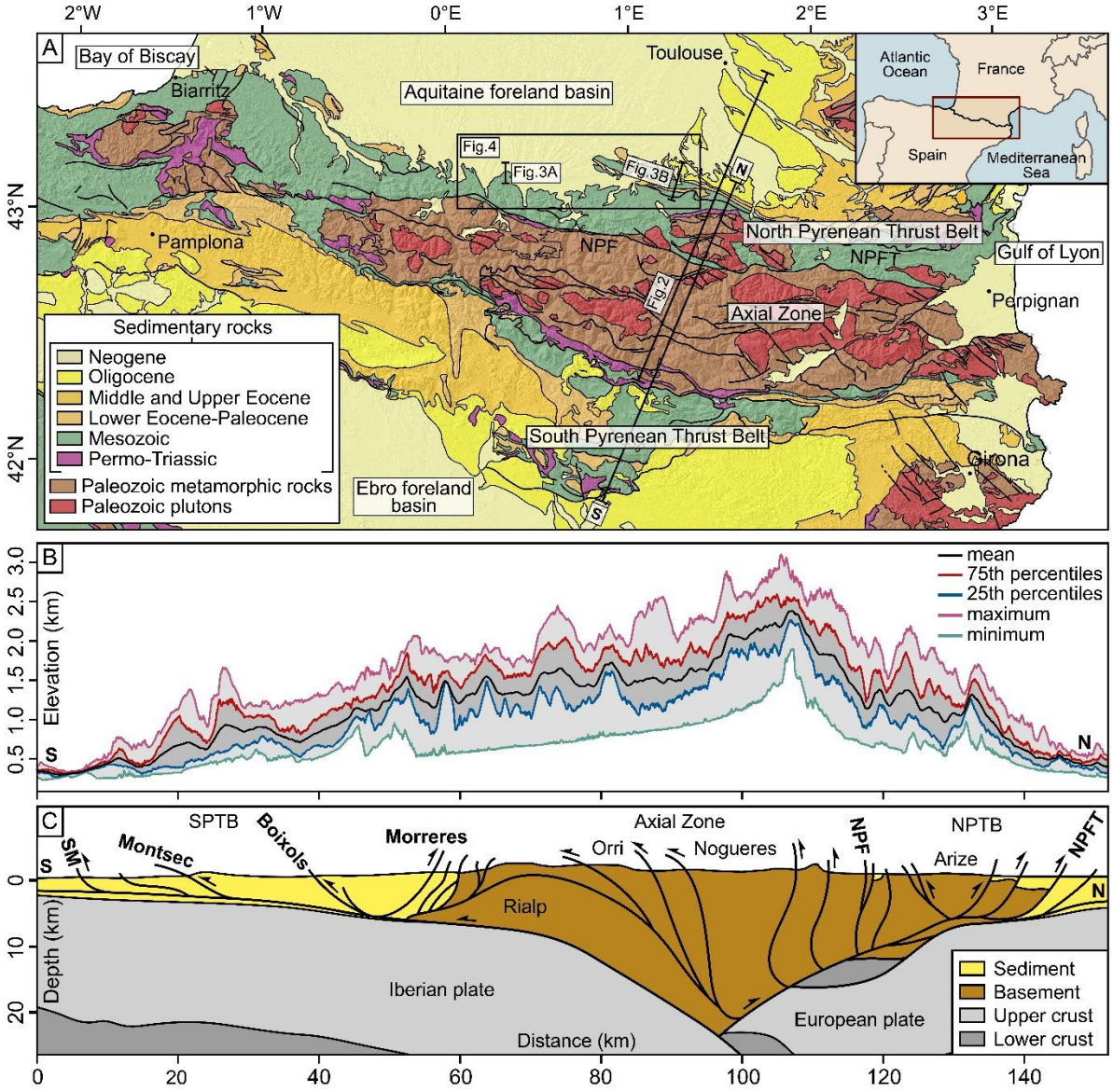

Figure 1. Geology of the Pyrenean system. A) Geologic map of the Pyrenees from the 1:1000000 BRGM geological map of France draped on a hillslope map from an SRTM digital topography with a resolution of 30 m. Black lines refer to locations of the elevation swath profile and geologic cross-section (panel B and C), the chronostratigraphic plot of Figure 2 and geologic cross-sections of Figure 3. Black square refers to the location of Figure 4. Cities are indicated by black dots. B) Swath profile of the central Pyrenees showing the mean (black lines), 75th percentile (red line), 25th percentile (blue line), maximum (magenta line) and minimum (cyan line) elevation. C) Simplified geologic cross-section of the central Pyrenees modified after Muñoz (1992); the distinction of basement and sediment relate to the contrasting densities used in the box model. NPF: North Pyrenean Fault. NPFT: North Pyrenean Frontal Thrust. SPTB: South Pyrenean Thrust Belt. NPTB: North Pyrenean Thrust Belt.

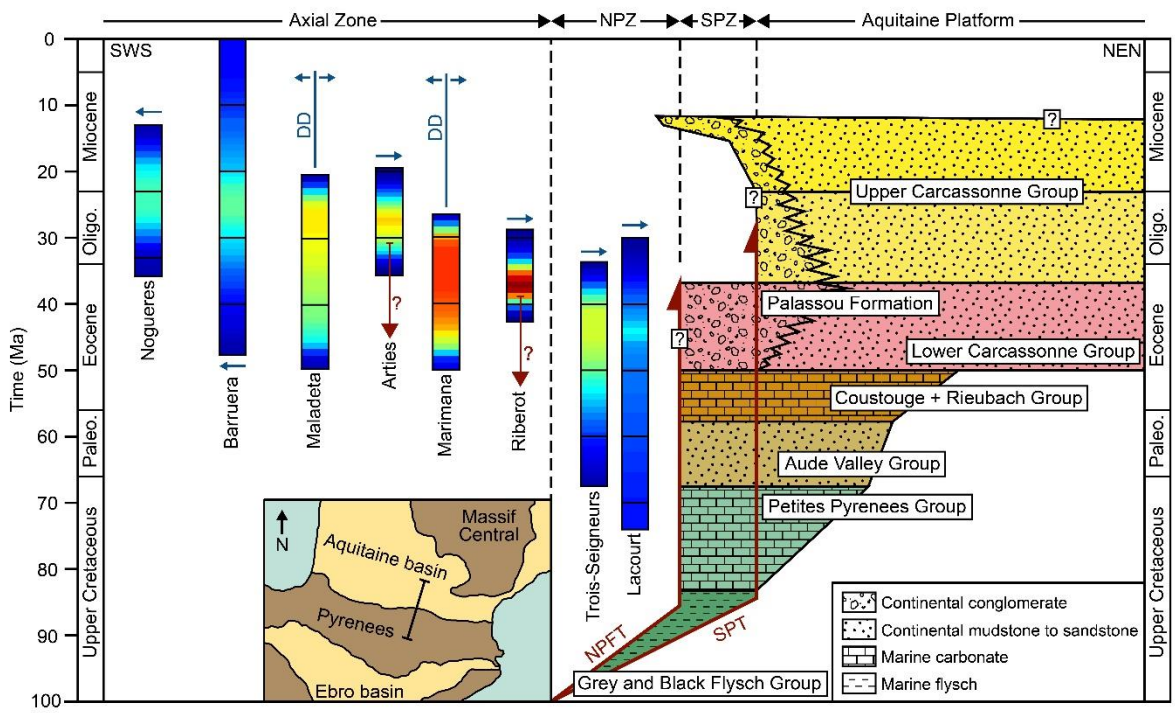

Figure 2. Relation between exhumation in the Pyrenean range and sedimentation in the north retro-foreland Aquitaine basin from Upper Cretaceous to Miocene time. Relative cooling rates based on thermochronology from Bernard et al., (2019) in the Axial Zone and North Pyrenean Zone is plotted (red: high cooling rate; blue: low cooling rate). Stratigraphy of the Aquitaine basin is adapted from Ford et al., (2015) and Rougier et al., (2016). Blue lines indicate the drainage divide position while blue arrows indicate flow water direction. Red lines indicate the main thrusts and their time of activity. NPFT: North Pyrenean Frontal Thrust. SPT: Sub-Pyrenean Thrust. NPZ: North Pyrenean Zone. SPZ: Sub-Pyrenean Zone.

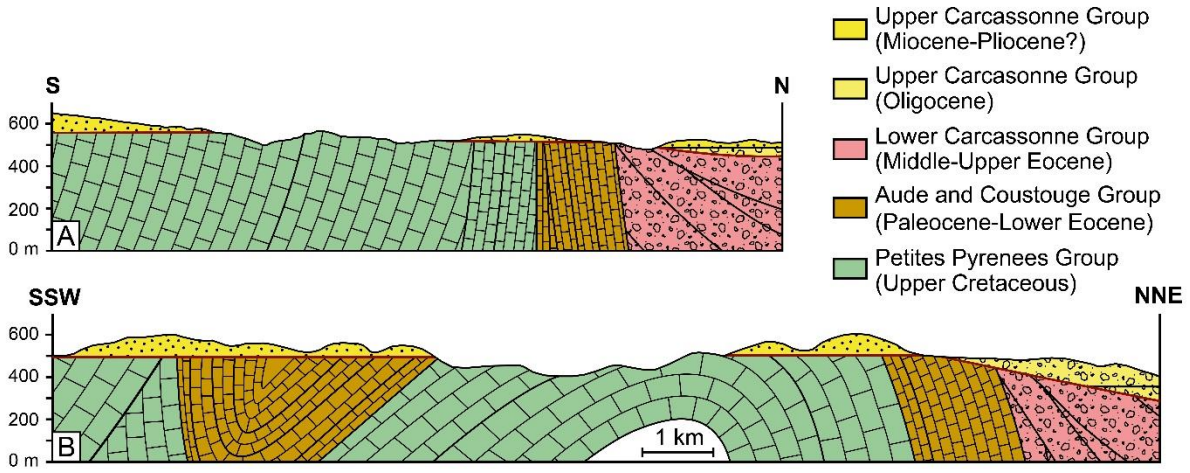

Figure 3. Geological cross-sections of the Central Northern Pyrenees showing draping by the Oligocene and Miocene sediments of eroded Pyrenean folds of the Sub-pyrenean Zone. A) Cross-section north to Bagneres-de-Bigorre from the 1:50000 BRGM geological map of Bagneres-de-Bigorre. B) Cross-section around St-Croix-Volvestre from the 1:50000 BRGM geological map of Le-Mas-d'Azil. Red lines on both cross-section highlight the stratigraphic unconformity recording the syn- to post-orogenic transition.

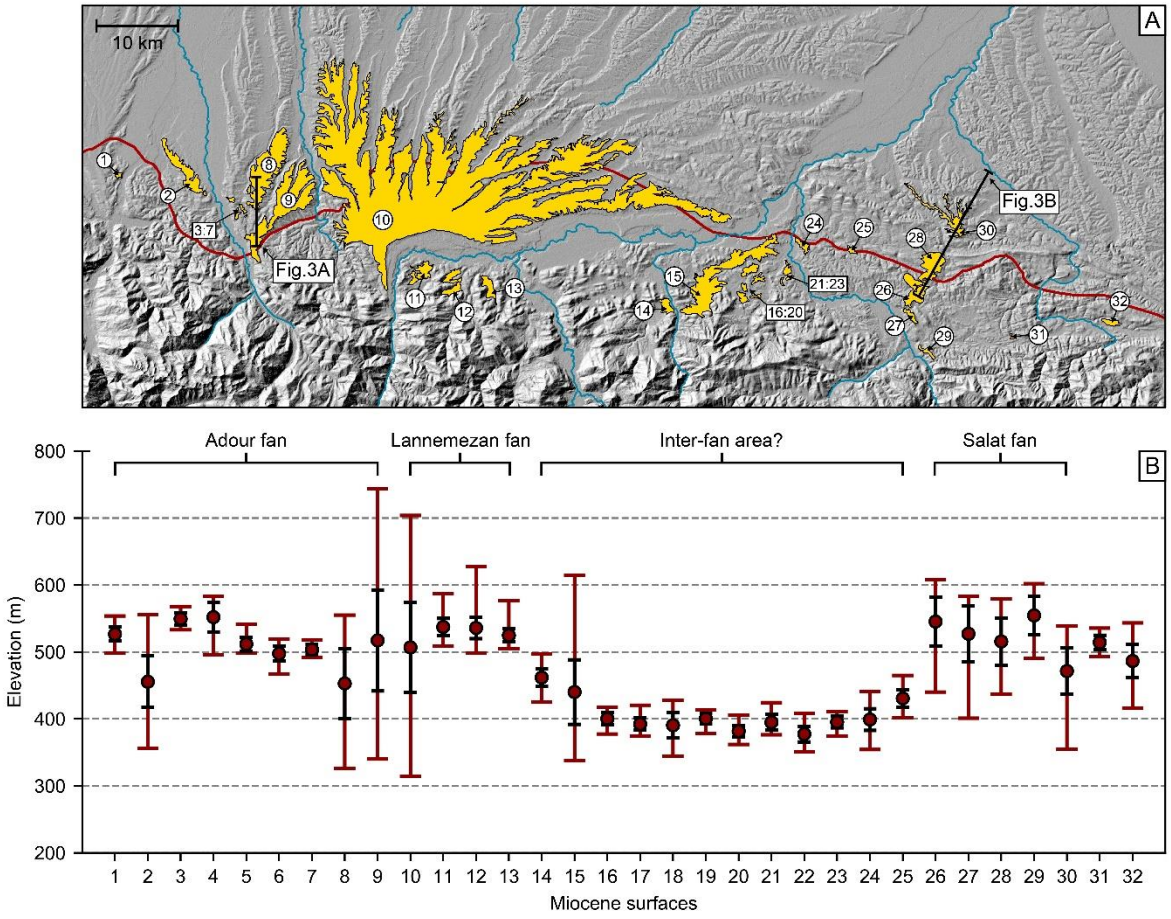

Figure 4. Miocene stratigraphic units of the northern Pyrenees at the boundary between the Aquitaine foreland basin and the Northern Pyrenean Thrust Belt highlighting their distribution across the Sub-Pyrenean Zone and North Pyrenean Zone. A) Middle Miocene-Pliocene surfaces (yellow areas) from the 1:50000 BRGM geologic map of Bagneres-de-Bigorre, Montrejeau, St-Gaudens, Le Mas-d'Azil, Aspet and St-Girons superimposed on a hillslope map from a SRTM with a resolution of 30 m. Black lines refer to locations of geologic cross-sections of Figure 3. B) Statistical elevation of the Miocene surfaces from West to East. The exact locations of the different Miocene surfaces are indicated in panel A. Red circles indicate the mean elevations. Black caps indicate the upper and lower standard deviations. Red caps indicate the maximum and minimum elevations.

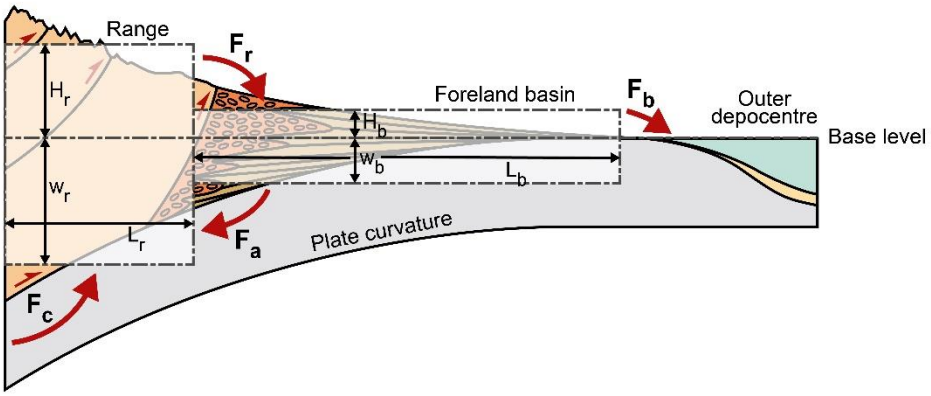

Figure 5. Cartoon summarising the main elements of the "box-model" modified after Tucker and van der Beek (2013). The orogenic system and associated foreland basin, shown schematically in the background are represented by two boxes, vertically positioned with respect to a horizontal base level that represents sea-level in this setting. F_r corresponds to the sediment flux from the range to the basin and F_b corresponds to the sediment flux from the basin to the outer depocentre. F_c corresponds to accretionary flux to the range due to plate convergence and underplating and F_a corresponds to accretionary flux from the basin to the range which in the case of many retro-wedge settings is negligible. All other parameters are defined in the text.

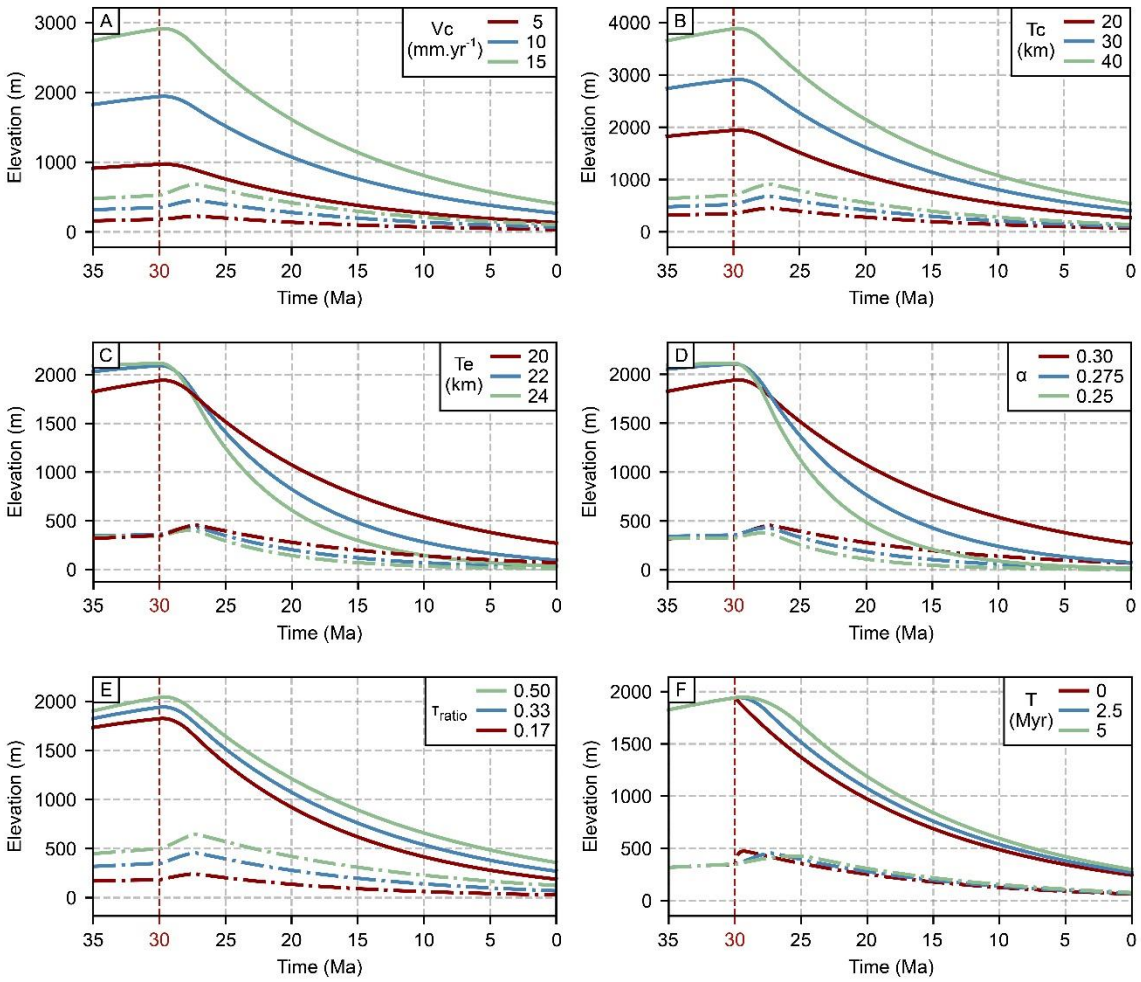

Figure 6. Effect of different parameters on the late syn- to post-orogenic mean elevation of a range (continuous lines) and adjacent foreland basin (dash lines). Convergence is active from 60 to 30 Ma and the transition from syn- to post-orogenesis is highlighted by a red vertical dashed line on each panel. The reference values that remain constant for the other models for each parameter is given in blue. A) Convergence velocity from 5 to 15 mm.yr^{-1}. B) Thickness of the accreted rock from 20 to 40 km. C) Lithosphere elastic thickness from 20 to 24 km. D) Relative proportion of the retro-wedge 0.25 to 0.30. E) Response time ratio between the range and foreland basin from 0.17 to 0.50. F) Time of convergence deceleration at the syn- to post-orogenic transition from 0 to 5 Ma.

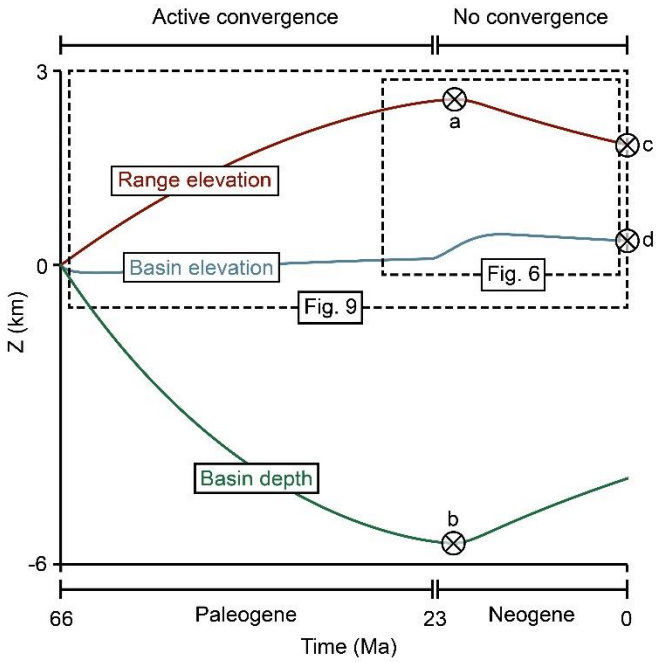

Figure 7. Schematic representation of the behaviour of measured parameters in the model during the evolution of an orogenic system from syn-orogenesis to post-orogenesis. For the Pyrenean case, active convergence occurred during Paleogene time. We highlight, with a circled x, the data from the model results that are compared with geologic data of the northern Pyrenees (a: maximum range elevation; b: depth of the basin at 23 Ma; c: present-day mean elevation of the range; d: present-day mean elevation of the basin). Note that for the generic experiments (Figure 6), the transition from active to no convergence is at 30 Ma. These schematic graphs are not to scale.

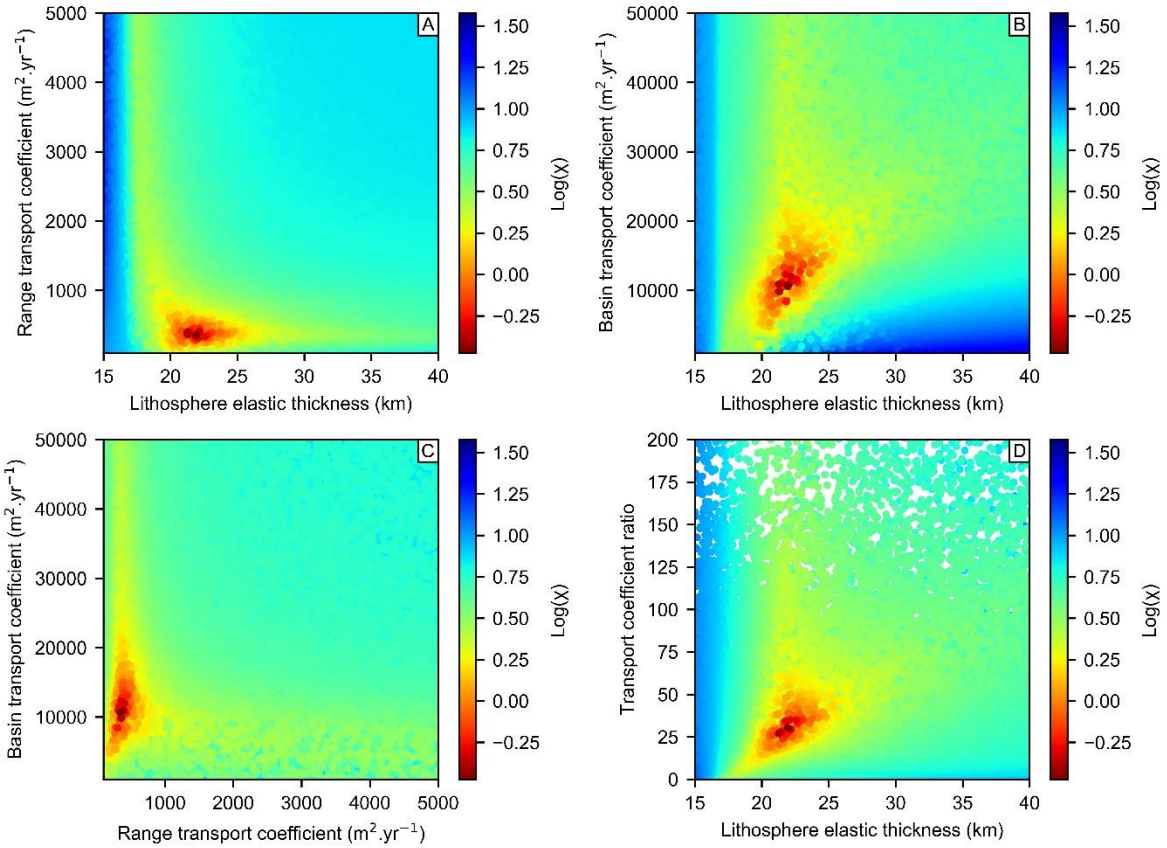

Figure 8. Misfit (χ) results of the different model outputs for three varying parameters (i.e. lithosphere elastic thickness, range and basin transport coefficient). Each circles correspond to a single model results with a total of 100,000 iterations. For panel A (lithosphere elastic thickness versus range transport coefficient), B (lithosphere elastic thickness versus basin transport coefficient) and C (range versus basin transport coefficient), the 3D space misfit is plotted as a function of two parameters with a mean interpolation of the third parameters. For panel D (lithosphere elastic thickness versus transport coefficient ratio), the misfit is represented in 2D. Lower misfit (better models) is represented by warmer colours and higher misfit (worse model) is represented by colder colours. Model results are accepted for a misfit lower than $\log(2) = 0.301$ (i.e. red to dark yellow dots).

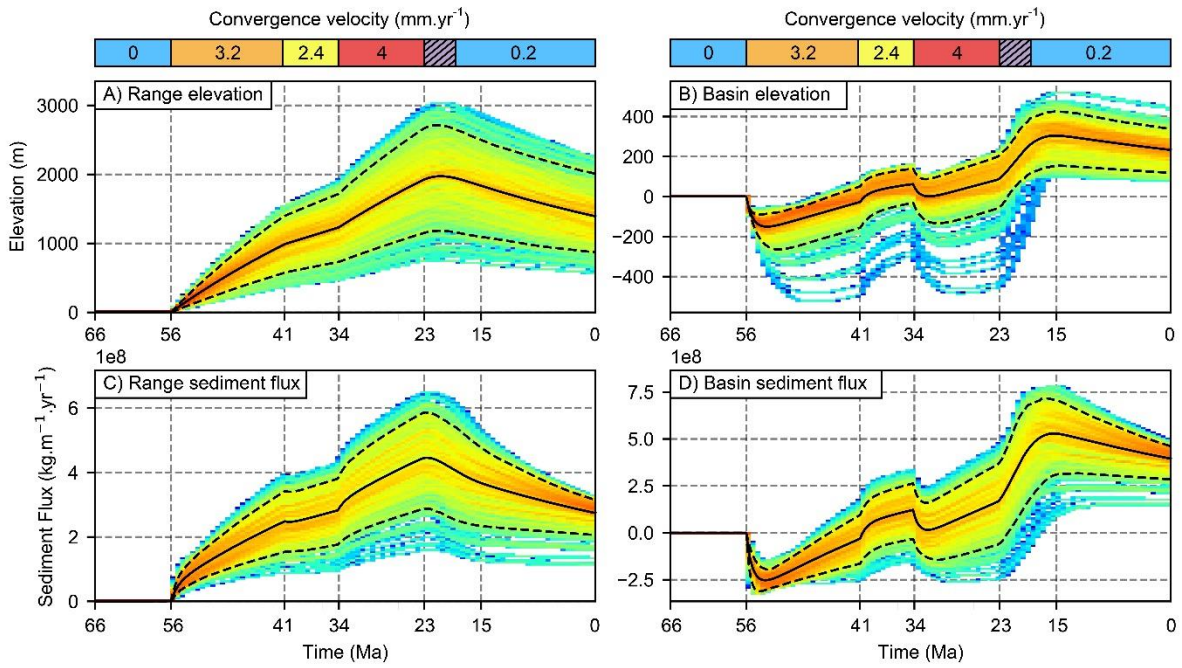

Figure 9. Model results for A) range elevation, B) basin elevation, C) sediment flux from the range to the basin and D) sediment flux from the basin to the outer basin through time. Colours correspond to the density model results with a misfit less than 0.15 from 100 000 iterations. Black lines correspond to the mean results while dash lines correspond to the upper and lower two standard deviations. Convergence velocity values through time are indicated above the four main panels. The purple dashed area indicates the phase of convergence deceleration starting at 23 Ma and lasting between 2.5 and 7.5 Myrs.

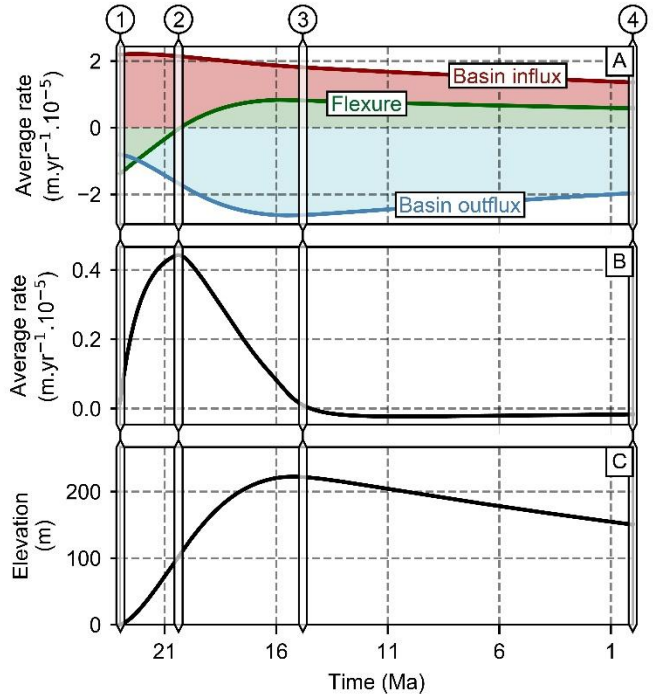

Figure 10. Contributions to the elevation of the foreland basin, inferred from the average result of accepted models, during the post-orogenic phase (i.e. 23 to 0 Ma) given as rates of range and basin sediment flux and basin flexure (A&B) and elevation (C) after cessation of active convergence. A) Contribution of different processes as rates through time. Red line corresponds to the sediment flux from the range to basin (basin influx). Blue line corresponds to the sediment flux from the basin to the outer basin (basin efflux). Basin outflux is negative as it contributes negatively to the elevation of the foreland basin. Green line corresponds to the flexure or vertical movement of the lithosphere or top basement (flexural subsidence or isostatic uplift). B) Basin elevation change evolution calculated as the sum of positive versus negative components in A. Positive or negative ratio means an increase or decrease respectively in elevation of the basin. C) Elevation accumulation of the basin through time from 23 to 0 Ma calculated from the integral of the average elevation change in panel B.

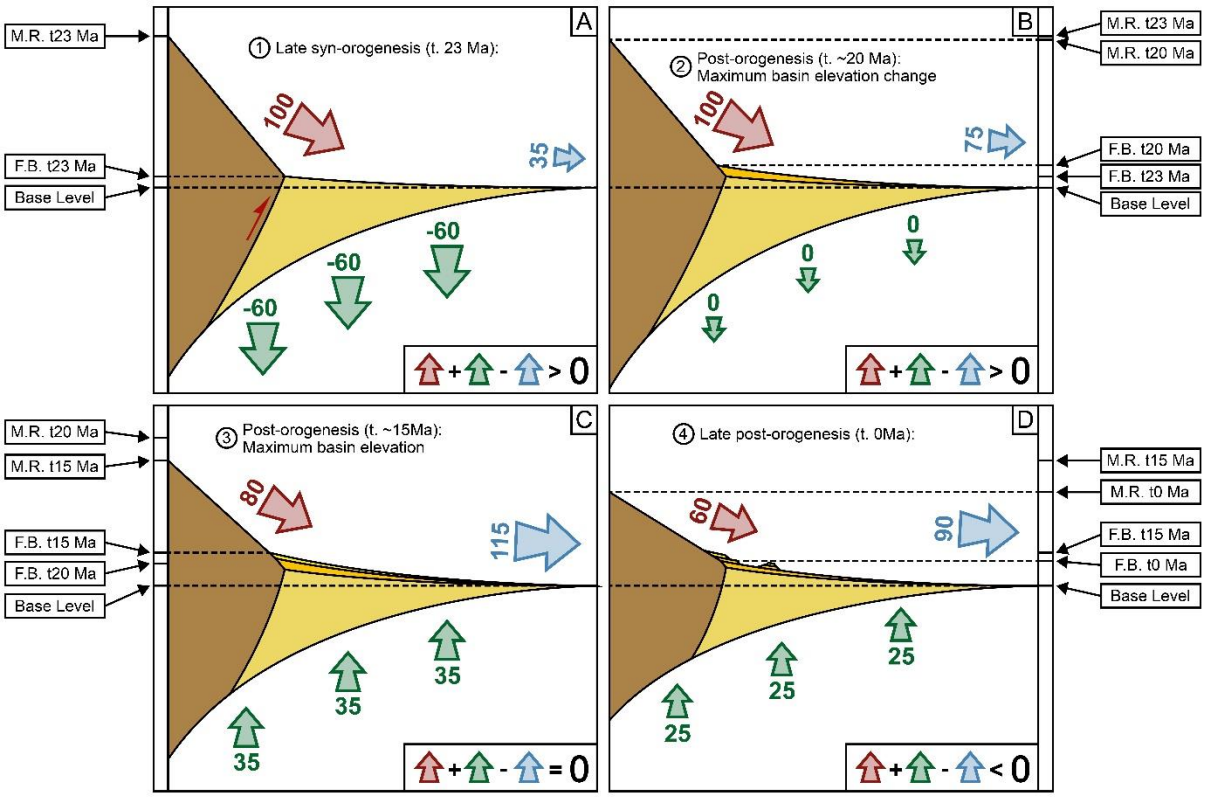

Figure 11. Schematic representation of the system evolution for four time frames during late syn- to post orogenesis. A) Late syn-orogenesis at 23 Ma. B) Early post-orogenesis at 20 Ma when positive elevation change of the foreland basin is maximum. C) Post-orogenesis at 15 Ma when elevation of the foreland basin is maximum. D) Post-orogenesis at 0 Ma when elevation of both the range and foreland basin are decreasing. Numbers for each time frame correspond to those in Figure 10 (i.e. 23, 20, 15 and 0 Ma). Red, green and blue arrows correspond respectively to the basin influx, lithospheric flexure and basin outflux with identical colours to those in Figure 10. Numbers next to the arrows indicate a percentage contribution to the basin elevation based on Figure 10. Black arrows indicate elevation of the range and foreland basin for the specific time frame and for the previous step for comparison.